

Anatomy of the differential gluon structure function of the proton from the experimental data on $F_{2p}(x, Q^2)$

I.P. Ivanov^{1,2,3*}, N.N. Nikolaev^{1,4†}

¹ IKP(Theorie), Forschungszentrum Jülich, Germany

² Institute of Mathematics, Novosibirsk, Russia

³ Novosibirsk State University, Novosibirsk, Russia

⁴L. D. Landau Institute for Theoretical Physics, Moscow, Russia

Abstract

The use of the differential gluon structure function of the proton $\mathcal{F}(x, Q^2)$ introduced by Fadin, Kuraev and Lipatov in 1975 is called upon in many applications of small- x QCD. We report here the first determination of $\mathcal{F}(x, Q^2)$ from the experimental data on the small- x proton structure function $F_{2p}(x, Q^2)$. We give convenient parameterizations for $\mathcal{F}(x, Q^2)$ based partly on the available DGLAP evolution fits (GRV, CTEQ & MRS) to parton distribution functions and on realistic extrapolations into soft region. We discuss an impact of soft gluons on various observables. The x -dependence of the so-determined $\mathcal{F}(x, Q^2)$ varies strongly with Q^2 and does not exhibit simple Regge properties. None the less the hard-to-soft diffusion is found to give rise to a viable approximation of the proton structure function $F_{2p}(x, Q^2)$ by the soft and hard Regge components with intercepts $\Delta_{soft} = 0$ and $\Delta_{hard} \sim 0.4$.

1 Introduction: Why unintegrated gluon structure functions?

The familiar objects from Gribov-Lipatov-Dokshitzer-Altarelli-Parisi (DGLAP) evolution description of deep inelastic scattering (DIS) are quark, antiquark and gluon distribution functions $q_i(x, Q^2)$, $\bar{q}(x, Q^2)$, $g(x, Q^2)$ (hereafter x, Q^2 are the standard DIS variables). At small x they describe the integral flux of partons with the lightcone momentum x in units of the target momentum and transverse momentum squared $\leq Q^2$ and form the basis of the highly sophisticated description of hard scattering processes in terms of collinear partons [1]. On the other hand, at very small x the object of the Balitskii-Fadin-Kuraev-Lipatov evolution equation is the differential gluon structure function (DGSF) of the target [2]

$$\mathcal{F}(x, Q^2) = \frac{\partial G(x, Q^2)}{\partial \log Q^2} \quad (1)$$

*E-mail: i.ivanov@fz-juelich.de

†E-mail: n.nikolaev@fz-juelich.de

(evidently the related unintegrated distributions can be defined also for charged partons). For instance, it is precisely DGSF of the target proton which emerges in the familiar color dipole picture of inclusive DIS at small x [3] and diffractive DIS into dijets [4]. Another familiar example is the QCD calculation of helicity amplitudes of diffractive DIS into continuum [5, 6] and production of vector mesons [7, 8]. DGSF's are custom-tailored for QCD treatment of hard processes, when one needs to keep track of the transverse momentum of gluons neglected in the standard collinear approximation [9].

In the past two decades DGLAP phenomenology of DIS has become a big industry and several groups — notably GRV [10], CTEQ [11] & MRS [12] and some other [13] — keep continuously incorporating new experimental data and providing the high energy community with updates of the parton distribution functions supplemented with the interpolation routines facilitating practical applications. On the other hand, there are several pertinent issues — the onset of the purely perturbative QCD treatment of DIS and the impact of soft mechanisms of photoabsorption on the proton structure function in the region of large Q^2 being top ones on the list — which can not be answered within the DGLAP approach itself because DGLAP evolution is obviously hampered at moderate to small Q^2 . The related issue is to what extent the soft mechanisms of photoabsorption can bias the Q^2 dependence of the proton structure function and, consequently, determination of the gluon density from scaling violations. We recall here the recent dispute [14] on the applicability of the DGLAP analysis at $Q^2 \lesssim 2\text{--}4 \text{ GeV}^2$ triggered by the so-called Caldwell's plot [15]. Arguably the κ -factorization formalism of DGSF in which the interesting observables are expanded in interactions of gluons of transverse momentum κ changing from soft to hard is better suited to look into the issue of soft-hard interface. At last but not the least, neglecting the transverse momentum κ of gluons is a questionable approximation in evaluation of production cross sections of jets or hadrons with large transverse momentum. It is distressing, then, that convenient parameterizations of DGSF are not yet available in the literature.

In this communication we report a simple phenomenological determination of the DGSF of the proton at small x . We analyze x and Q^2 dependence of the proton structure function $F_{2p}(x, Q^2)$ in the framework of the κ -factorization approach, which is closely related to the color dipole factorization. In the formulation of our Ansatz for $\mathcal{F}(x, \kappa^2)$ we take advantage of large body of the early work on color dipole factorization [3, 16, 17] and follow a very pragmatic strategy first applied in [5, 6]: (i) for hard gluons with large κ we make as much use as possible of the existing DGLAP parameterizations of $G(x, \kappa^2)$, (ii) for the extrapolation of hard gluon densities to small κ^2 we use an Ansatz [4] which correctly describes the color gauge invariance constraints on radiation of soft perturbative gluons by colour singlet targets, (iii) as suggested by color dipole phenomenology, we supplement the density of gluons with small κ^2 by nonperturbative soft component, (iv) as suggested by the soft-hard diffusion inherent to the BFKL evolution, we allow for propagation of the predominantly hard-interaction driven small- x rise of DGSF into the soft region invoking plausible soft-to-hard interpolations. The last two components of DGSF are parameterized following the modern wisdom on the infrared freezing of the QCD coupling and short propagation radius of perturbative gluons. Having specified the infrared regularization, we can apply the resulting $\mathcal{F}(x, \kappa^2)$ to evaluation of the photoabsorption cross section in the whole range of small to hard Q^2 .

The practical realization of the above strategy is expounded as follows: The subject of section 2 is a pedagogical introduction into the concept of DGSF on an example of Fermi-Weizsäcker-Williams photons in QED. Taking the electrically neutral positronium as a target,

we explain important constraints imposed by gauge invariance on DGSF at small κ^2 . In section 3 we present the κ -factorization approach, which is the basis of our analysis of small- x DIS in terms of DGSF. We also comment on the connection between the standard DGLAP analysis of DIS and κ -factorization and property of soft-to-hard and hard-to-soft diffusion inherent to κ -factorization. In section 4 we formulate our Ansatz for DGSF. The results of determination of DGSF from the experimental data on the proton structure function $F_{2p}(x, Q^2)$ and real photoabsorption cross section are presented in section 5. In section 6 we discuss an anatomy of the so-determined DGSF in the momentum space and comment on the interplay of soft and hard components in DGSF, integrated gluon SF and proton structure function $F_{2p}(x, Q^2)$. In section 7 we focus on effective intercepts of x -dependence, and the systematics of their change from DGSF to integrated gluon SF to $F_{2p}(x, Q^2)$, which illustrates nicely the gross features of soft-to-hard and hard-to-soft diffusion pertinent to BFKL physics. The subject of section 8 is a comparison of integrated gluon distributions from κ -factorization and conventional DGLAP analysis of the proton structure function. As anticipated, the two distributions diverge substantially at very small x and small to moderate Q^2 . In section 9 discuss in more detail how different observables — the scaling violations $\partial F_{2p}(x, Q^2)/\partial \log Q^2$, the longitudinal structure function $F_L(x, Q^2)$ and charm structure function $F_2^{c\bar{c}}(x, Q^2)$ — probe the DGSF. In section 10 we summarize our major findings.

2 Differential density of gauge bosons: the QED example

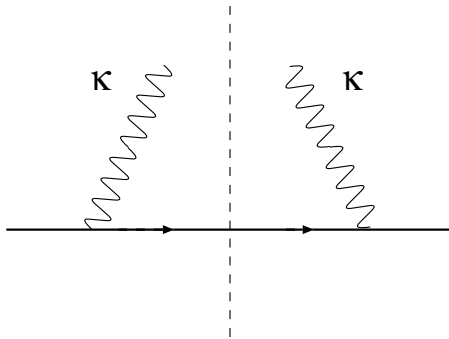


Figure 1: *The Fermi-Weizsäcker-Williams diagram for calculation of the flux of equivalent photons*

For the pedagogical introduction we recall the celebrated Fermi-Weizsäcker-Williams approximation in QED, which is the well known precursor of the parton model (for the review see [18]). Here high energy reactions in the Coulomb field of a charged particle are treated as collisions with equivalent transversely polarized photons — partons of the charged particle, fig.1. The familiar flux of comoving equivalent transverse soft photons carrying a lightcone fraction $x_\gamma \ll 1$ of the momentum of a relativistic particle, let it be the electron, reads

$$dn_e^\gamma = \frac{\alpha_{em}}{\pi} \frac{\kappa^2 d\kappa^2}{(\kappa^2 + \kappa_z^2)^2} \frac{dx_\gamma}{x_\gamma} \approx \frac{\alpha_{em}}{\pi} \frac{d\kappa^2}{\kappa^2} \frac{dx_\gamma}{x_\gamma}, \quad (2)$$

Here $\boldsymbol{\kappa}$ is photon transverse momentum and $\kappa_z = m_e x_\gamma$ is the photon longitudinal momentum in the electron Breit frame. The origin of $\boldsymbol{\kappa}^2$ in the numerator is in the current conservation, i.e. gauge invariance. Then the unintegrated photon structure function of the electron is by definition

$$\mathcal{F}_\gamma(x_\gamma, \boldsymbol{\kappa}^2) = \frac{\partial G_\gamma}{\partial \log \boldsymbol{\kappa}^2} = x_\gamma \frac{dn_e^\gamma}{dx_\gamma d \log \boldsymbol{\kappa}^2} = \frac{\alpha_{em}}{\pi} \left(\frac{\boldsymbol{\kappa}^2}{\boldsymbol{\kappa}^2 + \kappa_z^2} \right)^2. \quad (3)$$

If the relativistic particle is a positronium, fig. 2, destructive interference of electromagnetic fields of the electron and positron must be taken into account. Specifically, for soft photons with the wavelength $\lambda = \frac{1}{\kappa} \gg a_P$, where a_P is the positronium Bohr radius, the electromagnetic fields of an electron and positron cancel each other and the flux of photons vanishes, whereas for $\lambda \ll a_P$ the flux of photons will be twice that for a single electron. The above properties are quantified by the formula

$$\mathcal{F}_\gamma^P(x_\gamma, \boldsymbol{\kappa}^2) = 2 \frac{\alpha_{em}}{\pi} \left(\frac{\boldsymbol{\kappa}^2}{\boldsymbol{\kappa}^2 + \kappa_z^2} \right)^2 V(\kappa), \quad (4)$$

where the factor 2 is a number of charged particles in the positronium and corresponds to the Feynman diagrams of fig. 2a, 2b. The vertex function $V(\kappa)$ is expressed in terms of the two-body formfactor of the positronium,

$$V(\kappa) = 1 - F_2(\boldsymbol{\kappa}, -\boldsymbol{\kappa}) = 1 - \langle P | \exp(i\boldsymbol{\kappa}(\mathbf{r}_- - \mathbf{r}_+)) | P \rangle, \quad (5)$$

where $\mathbf{r}_- - \mathbf{r}_+$ is the spatial separation of e^+ and e^- in the positronium. The two-body formfactor $F_2(\boldsymbol{\kappa}, -\boldsymbol{\kappa})$ describes the destructive interference of electromagnetic fields of the electron and positron and corresponds to the Feynman diagrams of fig. 2c, 2d. It vanishes for large enough $\kappa \gtrsim a_P^{-1}$, leaving us with $V(\kappa) = 2$, whereas for soft gluons one has

$$V(\kappa) \propto \boldsymbol{\kappa}^2 a_P^2 \quad (6)$$

One can say that the law (6) is driven by electromagnetic gauge invariance, which guarantees that long wave photons decouple from the charge neutral system.

Finally, recall that the derivation of the differential flux of transverse polarized photons would equally hold if the photons were massive vector bosons interacting with the conserved current, the only change being in the propagator. For instance, for the charge neutral source one finds

$$\mathcal{F}_V^P(x_V, \boldsymbol{\kappa}^2) = \frac{\alpha_{em}}{\pi} \left(\frac{\boldsymbol{\kappa}^2}{\boldsymbol{\kappa}^2 + m_V^2} \right)^2 V(\kappa). \quad (7)$$

Recall that the massive vector fields are Yukawa-Debye screened with the screening radius

$$R_c = m_V^{-1}. \quad (8)$$

To the lowest in QED perturbation theory the two exchanged photons in figs. 1, 2 do not interact and we shall often refer to (7) as the Born approximation for the differential vector boson structure function. One can regard (7) as a minimal model for soft κ behavior of differential structure function for Yukawa-Debye screened vector bosons.

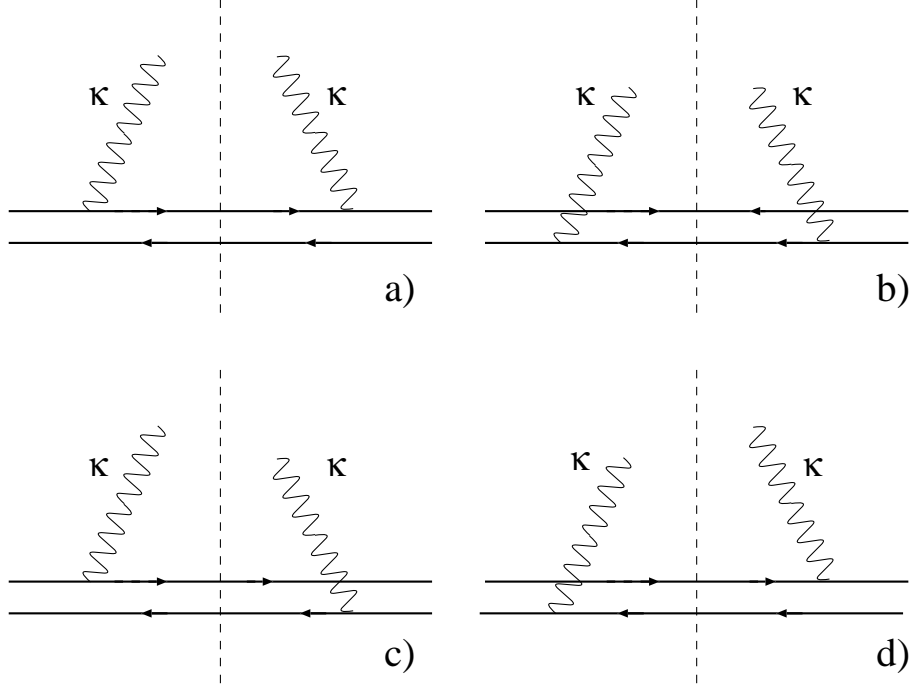


Figure 2: *The Fermi-Weizsäcker-Williams diagrams for calculation of the flux of equivalent photons in positronium.*

3 The insight into the differential density of gluons

3.1 Modeling virtual photoabsorption in QCD

The quantity which is measured in deep inelastic leptonproduction is the total cross section of photoabsorption $\gamma_{\mu}^*p \rightarrow X$ summed over all hadronic final states X , where $\mu, \nu = \pm 1, 0$ are helicities of (T) transverse and (L) longitudinal virtual photons. One usually starts with the imaginary part of the amplitude $A_{\mu\nu}$ of forward Compton scattering $\gamma_{\mu}^*p \rightarrow \gamma_{\nu}^*p'$, which by optical theorem gives the total cross section of photoabsorption of virtual photons

$$\sigma_T^{\gamma^*p}(x_{bj}, Q^2) = \frac{1}{\sqrt{(W^2 + Q^2 - m_p^2)^2 + 4Q^2m_p^2}} \text{Im}A_{\pm\pm}, \quad (9)$$

$$\sigma_L^{\gamma^*p}(x_{bj}, Q^2) = \frac{1}{\sqrt{(W^2 + Q^2 - m_p^2)^2 + 4Q^2m_p^2}} \text{Im}A_{00}, \quad (10)$$

where W is the total energy in the γ^*p *c.m.s.*, m_p is the proton mass, Q^2 is the virtuality of the photon and $x_{bj} = Q^2/(Q^2 + W^2 - m_p^2)$ is the Bjorken variable.

In perturbative QCD (pQCD) one models virtual photoabsorption in terms of the multiple production of gluons, quarks and antiquarks (fig. 3). The experimental integration over the full phase space of hadronic states X is substituted in the pQCD calculation by integration over the whole phase space of QCD partons

$$\int |M_{\mathcal{X}}|^2 d\tau_{\mathcal{X}} \Rightarrow \sum_n |M_n|^2 \prod \int_0^1 \frac{dx_i}{x_i} d^2\boldsymbol{\kappa}_i, \quad (11)$$

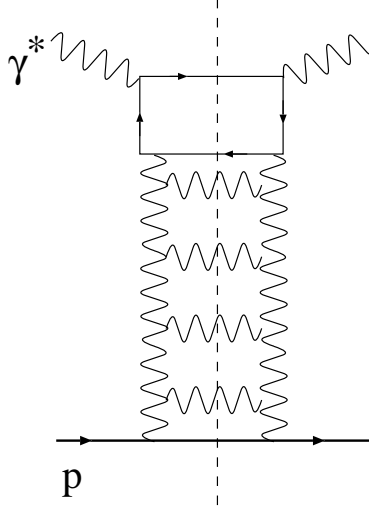


Figure 3: *The pQCD modeling of DIS in terms of multiproduction of parton final states.*

where the integration over the transverse momenta of partons goes over the whole allowed region

$$0 \leq \kappa_i^2 \leq \frac{1}{4}W^2 = \frac{Q^2(1-x)}{4x}. \quad (12)$$

The core of the so-called DGLAP approximation [1] is an observation that at finite x the dominant contribution to the multiparton production cross sections comes from a tiny part of the phase space

$$\begin{aligned} 1 &\geq x_1 \geq x_2 \dots \geq x_{n-1} \geq x_n \geq x & , \\ 0 &\leq \kappa_1^2 \ll \kappa_2^2 \dots \ll \kappa_{n-1}^2 \ll k^2 \ll Q^2 & , \end{aligned} \quad (13)$$

in which the upper limit of integration over transverse momenta of partons is much smaller than the kinematical limit (12). At very small x this limitation of the transverse phase space becomes much too restrictive and the DGLAP approximation is doomed to failure.

Hereafter we focus on how lifting the restrictions on the transverse phase space changes our understanding of the gluon structure function of the nucleon at very small x , that is, very large $\frac{1}{x}$. In this kinematical region the gluon density $g(x, Q^2)$ is much higher than the density of charged partons $q(x, Q^2), \bar{q}(x, Q^2)$. As Fadin, Kuraev and Lipatov [2] have shown, to the leading $\log \frac{1}{x}$ (LL $\frac{1}{x}$) approximation the dominant contribution to photoabsorption comes in this regime from multigluon final states of fig. 3; alternatively, to the LL $\frac{1}{x}$ splitting of gluons into gluons dominates the splitting of gluons into $q\bar{q}$ pairs. As a matter of fact, for the purposes of the present analysis we do not need the full BFKL dynamics, in the κ -factorization only the $q\bar{q}$ loop is treated explicitly to the LL $\frac{1}{x}$ approximation. In this regime the Compton scattering can be viewed as an interaction of the nucleon with the lightcone $q\bar{q}$ Fock states of the photon via the exchange by gluons, fig. 4, and the Compton scattering amplitude takes the form

$$A_{\nu\mu} = \Psi_{\nu, \lambda\bar{\lambda}}^* \otimes A_{q\bar{q}} \otimes \Psi_{\mu, \lambda\bar{\lambda}} \quad (14)$$

Here $\Psi_{\mu, \lambda\bar{\lambda}}$ is the Q^2 and q, \bar{q} helicity $\lambda, \bar{\lambda}$ dependent lightcone wave function of the photon and the QCD pomeron exchange $q\bar{q}$ -proton scattering kernel $A_{q\bar{q}}$ does not depend on, and conserves exactly, the q, \bar{q} helicities, summation over which is understood in (14).

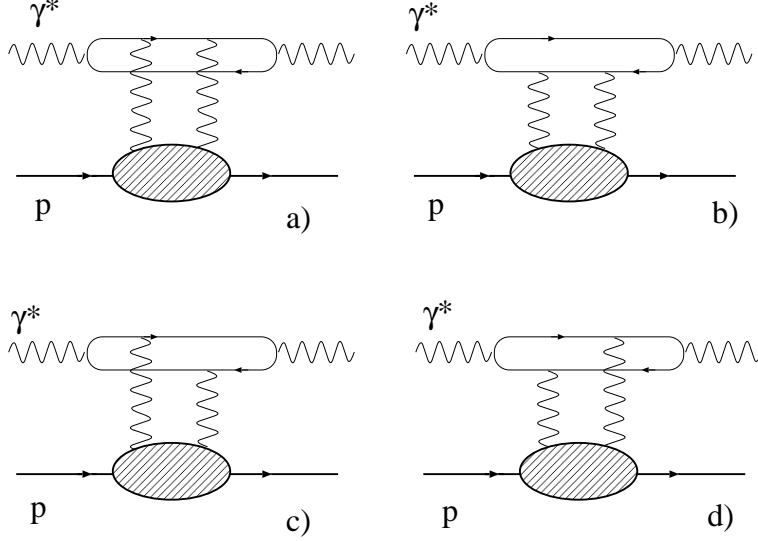


Figure 4: *The κ -factorization representation for DIS at small x .*

The resummation of diagrams of fig. 3 defines the unintegrated gluon structure function of the target, which is represented in diagrams of fig. 4 as the dashed blob. The calculation of the forward Compton scattering amplitudes ($\Delta = 0$) is straightforward and gives the κ -factorization formulas for photoabsorption cross sections [19, 20]

$$\begin{aligned} \sigma_T(x_{bj}, Q^2) &= \frac{\alpha_{em}}{\pi} \sum_f e_f^2 \int_0^1 dz \int d^2\mathbf{k} \int \frac{d^2\boldsymbol{\kappa}}{\boldsymbol{\kappa}^4} \alpha_S(q^2) \mathcal{F}(x_g, \boldsymbol{\kappa}^2) \\ &\quad \left\{ [z^2 + (1-z)^2] \left(\frac{\mathbf{k}}{\mathbf{k}^2 + \varepsilon^2} - \frac{\mathbf{k} - \boldsymbol{\kappa}}{(\mathbf{k} - \boldsymbol{\kappa})^2 + \varepsilon^2} \right)^2 \right. \\ &\quad \left. + m_f^2 \left(\frac{1}{\mathbf{k}^2 + \varepsilon^2} - \frac{1}{(\mathbf{k} - \boldsymbol{\kappa})^2 + \varepsilon^2} \right)^2 \right\} \end{aligned} \quad (15)$$

$$\begin{aligned} \sigma_L(x_{Bj}, Q^2) &= \frac{\alpha_{em}}{\pi} \sum_f e_f^2 \int_0^1 dz \int d^2\mathbf{k} \int \frac{d^2\boldsymbol{\kappa}}{\boldsymbol{\kappa}^4} \alpha_S(q^2) \mathcal{F}(x_g, \boldsymbol{\kappa}^2) \\ &\quad 4Q^2 z^2 (1-z)^2 \left(\frac{1}{\mathbf{k}^2 + \varepsilon^2} - \frac{1}{(\mathbf{k} - \boldsymbol{\kappa})^2 + \varepsilon^2} \right)^2 \end{aligned} \quad (16)$$

Here m_f and e_f are the mass and charge of the quark $f = u, d, s, c, b, \dots$,

$$\varepsilon^2 = z(1-z)Q^2 + m_f^2, \quad (17)$$

the QCD running coupling $\alpha_S(q^2)$ enters the integrand at the largest relevant virtuality,

$$q^2 = \max\{\varepsilon^2 + \mathbf{k}^2, \boldsymbol{\kappa}^2\}, \quad (18)$$

and the density of gluons enters at

$$x_g = \frac{Q^2 + M_t^2}{W^2 + Q^2} = x_{bj} \left(1 + \frac{M_t^2}{Q^2} \right). \quad (19)$$

Here M_t is the transverse mass of the produced $q\bar{q}$ pair in the photon-gluon fusion $\gamma^*g \rightarrow q\bar{q}$:

$$M_t^2 = \frac{m_f^2 + \mathbf{k}^2}{1-z} + \frac{m_f^2 + (\mathbf{k} - \boldsymbol{\kappa})^2}{z}. \quad (20)$$

For longitudinal photons only transitions $\gamma_L \rightarrow q_\lambda \bar{q}_{\bar{\lambda}}$ into states with $\lambda + \bar{\lambda} = 0$ are allowed. In σ_T the terms $\propto m_f^2$ are the contribution of states with $\lambda + \bar{\lambda} = \mu$, whereas the dominant contribution in the scaling regime of $Q^2 \gg m_f^2$ comes from the transitions $\gamma_T \rightarrow q_\lambda \bar{q}_{\bar{\lambda}}$ into states $\lambda + \bar{\lambda} = 0$, when the helicity of the photon is transferred to the angular momentum of the quark-antiquark pair. The corresponding transition amplitudes are $\propto \mathbf{k}, \mathbf{k} \pm \boldsymbol{\kappa}$, for more discussion see [7].

No restrictions on the transverse momentum in the $q\bar{q}$ loop, \mathbf{k} , and gluon momentum, $\boldsymbol{\kappa}$, are imposed in the representation (15), (16). This representation was contained essentially in the classic Fadin, Kuraev, Lipatov papers [2] of mid-70's, in the recent literature it is sometimes referred to as the $\boldsymbol{\kappa}$ -factorization.

We note that Eqs. (15), (16) are for forward diagonal Compton scattering, but similar representation in terms of the unintegrated gluons structure function holds also for the off-forward Compton scattering at finite momentum transfer $\boldsymbol{\Delta}$, off-diagonal Compton scattering when the virtualities of the initial and final state photons are different, $Q_f^2 \neq Q_i^2$, including the timelike photons and vector mesons, $Q_f^2 = -m_V^2$, in the final state.

The photoabsorption cross sections define the dimensionless structure functions

$$F_{T,L}(x_{bj}, Q^2) = \frac{Q^2}{4\pi^2\alpha_{em}}\sigma_{T,L} \quad (21)$$

and $F_2 = F_T + F_L$, which admit the familiar pQCD parton model interpretation

$$F_T(x_{bj}, Q^2) = \sum_{f=u,d,s,c,b,\dots} e_f^2 [q_f(x_{bj}, Q^2) + \bar{q}_f(x_{bj}, Q^2)], \quad (22)$$

where $q_f(x_{bj}, Q^2), \bar{q}_f(x_{bj}, Q^2)$ are the integrated density of quarks and antiquarks carrying the fraction x_{bj} of the lightcone momentum of the target and with transverse momenta $\leq Q$. Hereafter we suppress the subscript "bj".

3.2 Where $\boldsymbol{\kappa}_\perp$ -factorization meets DGLAP factorization

Recall the familiar DGLAP equation [1] for scaling violations at small x ,

$$\frac{dF_2(x, Q^2)}{d \log Q^2} = \sum_f e_f^2 \frac{\alpha_S(Q^2)}{2\pi} \int_x^1 dy [y^2 + (1-y)^2] G\left(\frac{x}{y}, Q^2\right) \approx \frac{\alpha_S(Q^2)}{3\pi} G(2x, Q^2) \sum_f e_f^2, \quad (23)$$

where for the sake of simplicity we only consider light flavours. Upon integration we find

$$F_2(x, Q^2) \approx \sum_f e_f^2 \int_0^{Q^2} \frac{d\bar{Q}^2}{\bar{Q}^2} \frac{\alpha_S(\bar{Q}^2)}{3\pi} G(2x, \bar{Q}^2). \quad (24)$$

In order to see the correspondence between the $\boldsymbol{\kappa}_\perp$ -factorization and DGLAP factorization it is instructive to follow the derivation of (24) from the $\boldsymbol{\kappa}_\perp$ -representation (15).

First, separate the κ^2 -integration in (15) into the DGLAP part of the gluon phase space $\kappa^2 \lesssim \bar{Q}^2 = \epsilon^2 + k^2$ and beyond-DGLAP region $\kappa^2 \gtrsim \bar{Q}^2$. One readily finds

$$\left(\frac{\mathbf{k}}{k^2 + \epsilon^2} - \frac{\mathbf{k} - \boldsymbol{\kappa}}{(\mathbf{k} - \boldsymbol{\kappa})^2 + \epsilon^2} \right)^2 = \begin{cases} \left(\frac{2z^2(1-z)^2Q^4}{\bar{Q}^8} - \frac{2z(1-z)Q^2}{\bar{Q}^6} + \frac{1}{\bar{Q}^4} \right) \boldsymbol{\kappa}^2 & \text{if } \boldsymbol{\kappa}^2 \ll \bar{Q}^2 \\ \left(\frac{1}{\bar{Q}^2} - \frac{z(1-z)Q^2}{\bar{Q}^4} \right), & \text{if } \boldsymbol{\kappa}^2 \gtrsim \bar{Q}^2 \end{cases} \quad (25)$$

Consider first the contribution from the DGLAP part of the phase space $\kappa^2 \lesssim \bar{Q}^2$. Notice that because of the factor $\boldsymbol{\kappa}^2$ in (25), the straightforward $\boldsymbol{\kappa}^2$ integration of the DGLAP component yields $G(x_g, \bar{Q}^2)$ and \bar{Q}^2 is precisely the pQCD hard scale for the gluonic transverse momentum scale:

$$\begin{aligned} & \int_0^{\bar{Q}^2} \frac{d\boldsymbol{\kappa}^2}{\boldsymbol{\kappa}^2} \alpha_S(q^2) \mathcal{F}(x_g, \boldsymbol{\kappa}^2) \left(\frac{\mathbf{k}}{k^2 + \epsilon^2} - \frac{\mathbf{k} - \boldsymbol{\kappa}}{(\mathbf{k} - \boldsymbol{\kappa})^2 + \epsilon^2} \right)^2 \\ &= \left(\frac{2z^2(1-z)^2Q^4}{\bar{Q}^8} - \frac{2z(1-z)Q^2}{\bar{Q}^6} + \frac{1}{\bar{Q}^4} \right) G(x_g, \bar{Q}^2) \end{aligned} \quad (26)$$

The contribution from the beyond-DGLAP region of the phase space can be evaluated as

$$\begin{aligned} & \int_{\bar{Q}^2}^{\infty} \frac{d\boldsymbol{\kappa}^2}{\boldsymbol{\kappa}^4} \alpha_S(q^2) \mathcal{F}(x_g, \boldsymbol{\kappa}^2) \left(\frac{1}{\bar{Q}^2} - \frac{z(1-z)Q^2}{\bar{Q}^4} \right) = \left(\frac{1}{\bar{Q}^4} - \frac{z(1-z)Q^2}{\bar{Q}^6} \right) \mathcal{F}(x_g, \bar{Q}^2) I(x_g, \bar{Q}^2) \\ &= \left(\frac{2z^2(1-z)^2Q^4}{\bar{Q}^8} - \frac{2z(1-z)Q^2}{\bar{Q}^6} + \frac{1}{\bar{Q}^4} \right) \mathcal{F}(x_g, \bar{Q}^2) \log C_2(x_g, \bar{Q}^2, z). \end{aligned} \quad (27)$$

The latter form of (27) allows to conveniently combine (26) and (27) rescaling the hard scale in the GSF

$$G(x_g, \bar{Q}^2) + \mathcal{F}(x_g, \bar{Q}^2) \log C_2(x_g, \bar{Q}^2, z) = G(x_g, C_2(x_g, \bar{Q}^2, z) \bar{Q}^2). \quad (28)$$

Here the exact value of $I(x_g, \bar{Q}^2) \geq 1$ depends on the rate of the $\boldsymbol{\kappa}^2$ -rise of $\mathcal{F}(x_g, \boldsymbol{\kappa}^2)$. At small x_g and small to moderate \bar{Q}^2 one finds $I(x_g, \bar{Q}^2)$ substantially larger than 1 and $C_2(x_g, \bar{Q}^2, z) \gg 1$, see more discussion below in section 9.

Now change from $d\boldsymbol{\kappa}^2$ integration to $d\bar{Q}^2$ and again split the z, Q^2 integration into the DGLAP part of the phase space $\bar{Q}^2 \ll \frac{1}{4}Q^2$, where either $z < \frac{\bar{Q}^2}{Q^2}$ or $1-z < \frac{\bar{Q}^2}{Q^2}$, and the beyond-DGLAP region $\bar{Q}^2 \gtrsim \frac{1}{4}Q^2$, where $0 < z < 1$. As a result one finds

$$\begin{aligned} & \int dz [z^2 + (1-z)^2] \left(\frac{2z^2(1-z)^2Q^4}{\bar{Q}^8} - \frac{2z(1-z)Q^2}{\bar{Q}^6} + \frac{1}{\bar{Q}^4} \right) \\ &= \begin{cases} \frac{4}{3\bar{Q}^2Q^2}, & \text{if } \bar{Q}^2 \ll \frac{1}{4}Q^2 \\ \left(2A_2 \frac{Q^4}{\bar{Q}^8} - 2A_1 \frac{Q^2}{\bar{Q}^6} + A_0 \frac{1}{\bar{Q}^4} \right), & \text{if } \bar{Q}^2 \gtrsim \frac{1}{4}Q^2 \end{cases} \end{aligned} \quad (29)$$

where

$$A_m = \int_0^1 dz [z^2 + (1-z)^2] z^m (1-z)^m \quad (30)$$

Let \bar{C}_2 be $C_2(x_g, \bar{Q}^2, z)$ at a mean point. Notice also that $M_t^2 \sim Q^2$, so that $x_g \sim 2x$. Then the contribution from the DGLAP phase space of \bar{Q}^2 can be cast in precisely the form (24)

$$F_2(x, Q^2)|_{DGLAP} \approx \sum_f e_f^2 \int_0^{\bar{C}_2 Q^2} \frac{d\bar{Q}^2}{\bar{Q}^2} \frac{\alpha_S(\bar{Q}^2)}{3\pi} G(2x, \bar{Q}^2). \quad (31)$$

The beyond-DGLAP region of the phase space gives the extra contribution of the form

$$\begin{aligned} \Delta F_2(x, Q^2)|_{non-DGLAP} &\sim \sum_f e_f^2 \frac{\alpha_S(Q^2)}{3\pi} \int_{Q^2}^{\infty} \frac{d\bar{Q}^2}{\bar{Q}^2} \frac{Q^2}{\bar{Q}^2} G(2x, \bar{Q}^2) \\ &\sim \sum_f e_f^2 \frac{\alpha_S(Q^2)}{3\pi} G(2x, Q^2). \end{aligned} \quad (32)$$

Eqs.(31) and (32) immediately reveal the phenomenological consequences of lifting the DGLAP restrictions in the transverse momenta integration. Indeed, the DGLAP approach respects the following strict inequalities

$$\kappa^2 \ll \mathbf{k}^2 \quad \text{and} \quad \mathbf{k}^2 \ll Q^2. \quad (33)$$

As we just saw, removing the first limitation effectively shifted the upper limit in the \bar{Q}^2 integral to $\bar{C}_2 Q^2 \neq Q^2$, while lifting the second constraint led to an additional, purely non-DGLAP contribution. Although both of these corrections lack one leading $\log-Q^2$ factor they are numerically substantial. As a matter of fact, in section 9 we show that $\bar{C}_2 \approx 8$.

The above analysis suggests that the DGLAP and κ -factorization schemes converge logarithmically at large Q^2 . However, in order to reproduce the result (31) and (32) for the full phase space by the conventional DGLAP contribution (24) from the restricted phase space (13) one has to ask for DGLAP gluon density $G_{pt}(x, Q^2)$ larger than the integrated GSF in the κ -factorization scheme and the difference may be quite substantial in the domain of strong scaling violations.

3.3 The different evolution paths: soft-to-hard diffusion and vice versa

The above discussion of the contributions to the total cross section from the DGLAP and non-DGLAP parts of the phase space can conveniently be cast in the form of the Huygens principle. To the standard DGLAP leading $\log Q^2$ (LL Q^2) approximation one only considers the contribution from the restricted part of the available transverse phase space (13). The familiar Huygens principle for the homogeneous DGLAP LL Q^2 evaluation of parton densities in the x_{bj} - Q^2 plane is illustrated in fig. 5a: one starts with the boundary condition $p(x, Q_0^2)$ as a function of x at fixed Q_0^2 , the evolution paths (z, \tilde{Q}^2) for the calculation of $p(x, Q^2)$ shown in fig. 5a are confined to a rectangle $x \leq z \leq 1$, $Q_0^2 \leq \tilde{Q}^2 \leq Q^2$, the evolution is unidirectional in the sense that there is no feedback on the x -dependence of $p(x, Q_1^2)$ from the x -dependence of $p(x, Q_2^2)$ at $Q_2^2 \geq Q_1^2$. In fig. 5a we show some examples of evolution paths which are kinematically allowed but neglected in the DGLAP approximation. Starting with about flat or slowly rising $G(x, Q_0^2)$ one finds that the larger Q^2 , the steeper the small- x rise of $G(x, Q^2)$.

At $x \ll 1$ the DGLAP contribution from the restricted transverse phase space (13) no longer dominates the multiparton production cross sections, the restriction (13) must be lifted

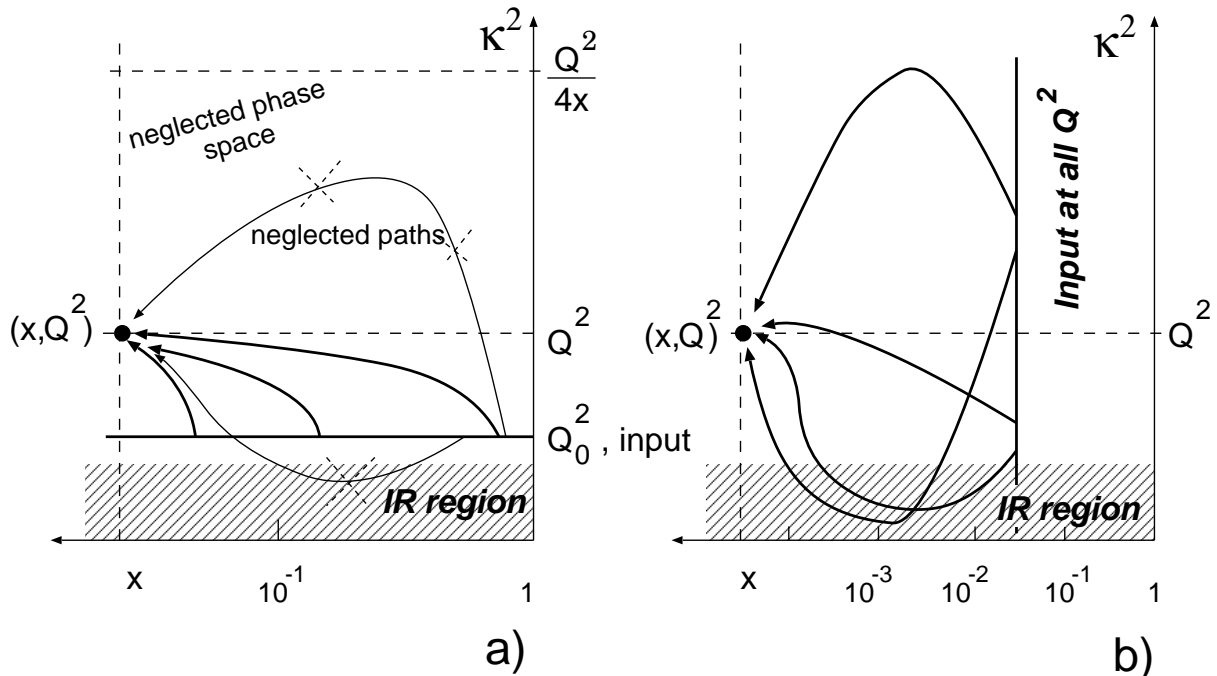


Figure 5: *The Huygens principle for Q^2, x evolution of DIS structure functions with (a) DGLAP restricted transverse phase space and (b) for the BFKL x evolution without restrictions on the transverse phase space and hard-to-soft & soft-to-hard diffusion.*

and the contribution to the cross section from small κ_i^2 and large $\kappa_i^2 \gtrsim Q^2$ can no longer be neglected. The Huygens principle for the homogeneous BFKL evolution is illustrated in fig. 5b: one starts with the boundary condition $\mathcal{F}(x_0, Q^2)$ as a function of Q^2 at fixed $x_0 \ll 1$, the evolution paths (z, \tilde{Q}^2) for the calculation of $p(x, Q^2)$ are confined to a stripe $x \leq z \leq x_0$, in contrast the the unidirectional DGLAP evolution one can say that under BFKL evolution the small- x behaviour of $p(x, Q^2)$ at large Q^2 is fed partly by the x -dependence of soft $p(x, Q^2)$ at larger x and vice versa. The most dramatic consequence of this soft-to-hard and hard-to-soft diffusion which can not be eliminated is that at very small x the x -dependence of the gluon structure in the soft and hard regions will eventually be the same:

$$\lim_{\frac{1}{x} \rightarrow \infty} G(x, Q^2) = G(Q^2) \left(\frac{1}{x}\right)^{\Delta_{\mathbf{P}}} . \quad (34)$$

The rate of such a hard-to-soft diffusion is evidently sensitive to the infrared regularization of pQCD, the model estimates show that in the HERA range of x it is very slow [21, 22].

4 The Ansatz for differential gluon structure function

The major insight into parameterization of DGSF comes from early experience with color dipole phenomenology of small- x DIS. In color dipole approach, which is closely related to κ -factorization, the principal quantity is the total cross section of interaction of the $q\bar{q}$ color

dipole \mathbf{r} with the proton target [3, 20, 23]

$$\sigma(x, r) = \frac{\pi^2 r^2}{3} \int \frac{d\boldsymbol{\kappa}^2}{\boldsymbol{\kappa}^2} \frac{4[1 - J_0(\kappa r)]}{(\kappa r)^2} \alpha_S \left(\max\{\boldsymbol{\kappa}^2, \frac{A}{r^2}\} \right) \mathcal{F}(x, \boldsymbol{\kappa}^2), \quad (35)$$

which for very small color dipoles can be approximated by

$$\sigma(x, r) = \frac{\pi^2 r^2}{3} \alpha_S \left(\frac{A}{r^2} \right) G \left(x, \frac{A}{r^2} \right), \quad (36)$$

where $A \approx 10$ comes from properties of the Bessel function $J_0(z)$. The phenomenological properties of the dipole cross section are well understood, for extraction of $\sigma(x, r)$ from the experimental data see [24, 25]. The known dipole size dependence of $\sigma(x, r)$ serves as a constrain on the possible $\boldsymbol{\kappa}^2$ -dependence of $\mathcal{F}(x, \boldsymbol{\kappa}^2)$.

As we argued in section 3.2, DGLAP fits are likely to overestimate $\mathcal{F}_{hard}(x, \boldsymbol{\kappa}^2)$ at moderate $\boldsymbol{\kappa}^2$. Still, approximation (36) does a good job when the hardness A/r^2 is very large, and at large Q^2 we can arguably approximate the DGSF by the direct differentiation of available fits (GRV, CTEQ, MRS, ...) to the integrated gluon structure function $G_{pt}(x, Q^2)$:

$$\mathcal{F}_{pt}(x, \boldsymbol{\kappa}^2) \approx \frac{\partial G_{pt}(x, \boldsymbol{\kappa}^2)}{\partial \log \boldsymbol{\kappa}^2} \quad (37)$$

Hereafter the subscript pt serves as a reminder that these gluon distributions were obtained from the pQCD evolution analyses of the proton structure function and cross sections of related hard processes.

The available DGLAP fits are only applicable at $\boldsymbol{\kappa}^2 \geq Q_c^2$, see table 1 for the values of Q_c^2 , in the extrapolation to soft region $\boldsymbol{\kappa}^2 \leq Q_c^2$ we are bound to educated guess. To this end recall that perturbative gluons are confined and do not propagate to large distances; recent fits [26] to the lattice QCD data suggest Yukawa-Debye screening of perturbative color fields with propagation/screening radius $R_c \approx 0.27 fm$. Incidentally, precisely this value of R_c for Yukawa screened colour fields has been used since 1994 in the very successful color dipole phenomenology of small- x DIS [16, 17]. Furthermore, important finding of [17] is a good quantitative description of the rising component of the proton structure function starting with the Yukawa-screened perturbative two-gluon exchange as a boundary condition for the color dipole BFKL evolution.

The above suggests that $\boldsymbol{\kappa}^2$ dependence of perturbative hard $\mathcal{F}_{hard}(x, \boldsymbol{\kappa}^2)$ in the soft region $\boldsymbol{\kappa}^2 \leq Q_c^2$ is similar to the Yukawa-screened flux of photons in the positron, cf. eq. (4), with α_{em} replaced by the running strong coupling of quarks $C_F \alpha_S(\boldsymbol{\kappa}^2)$ and with factor N_c instead of 2 leptons in the positronium, for the early discussion see [4],

$$\mathcal{F}_{pt}^{(B)}(\boldsymbol{\kappa}^2) = C_F N_c \frac{\alpha_S(\boldsymbol{\kappa}^2)}{\pi} \left(\frac{\boldsymbol{\kappa}^2}{\boldsymbol{\kappa}^2 + \mu_{pt}^2} \right)^2 V_N(\boldsymbol{\kappa}), \quad (38)$$

Here $\mu_{pt} = \frac{1}{R_c} = 0.75$ GeV is the inverse Yukawa screening radius and must not be interpreted as a gluon mass; more sophisticated forms of screening can well be considered. Following [16, 17, 19, 21] we impose also the infrared freezing of strong coupling: $\alpha_S(\boldsymbol{\kappa}^2) \leq 0.82$; recently the concept of freezing coupling has become very popular, for the review see [28].

The vertex function $V_N(\boldsymbol{\kappa})$ describes the decoupling of soft gluons, $\boldsymbol{\kappa} \ll \frac{1}{R_p}$, from color neutral proton and has the same structure as in eq. (5). In the nonrelativistic oscillator model

for the nucleon one can relate the two-quark form factor of the nucleon to the single-quark form factor,

$$F_2(\vec{\kappa}, -\vec{\kappa}) = F_1\left(\frac{2N_c}{N_c - 1}\kappa^2\right). \quad (39)$$

To the extent that $R_c^2 \ll R_p^2$ the detailed functional form of $F_2(\vec{\kappa}, -\vec{\kappa})$ is not crucial, the simple relation (39) will be used also for a more realistic dipole approximation

$$F_1(\kappa^2) = \frac{1}{\left(1 + \frac{\kappa^2}{\Lambda^2}\right)^2}. \quad (40)$$

The gluon probed radius of the proton and the charge radius of the proton can be somewhat different and $\Lambda \sim 1$ GeV must be regarded as a free parameter. Anticipating the forthcoming discussion of the diffraction slope in vector meson production we put $\Lambda = 1$ GeV.

As discussed above, the hard-to-soft diffusion makes the DGSF rising at small- x even in the soft region. We model this hard-to-soft diffusion by matching the κ^2 dependence (38) to the DGLAP fit $\mathcal{F}_{pt}(x, Q_c^2)$ at the soft-hard interface Q_c^2 and assigning to $\mathcal{F}_{hard}(x, \kappa^2)$ in the region of $\kappa^2 \leq Q_c^2$ the same x -dependence as shown by the DGLAP fit $\mathcal{F}_{pt}(x, Q_c^2)$, i.e.,

$$\mathcal{F}_{hard}(x, \kappa^2) = \mathcal{F}_{pt}^{(B)}(\kappa^2) \frac{\mathcal{F}_{pt}(x, Q_c^2)}{\mathcal{F}_{pt}^{(B)}(Q_c^2)} \theta(Q_c^2 - \kappa^2) + \mathcal{F}_{pt}(x, \kappa^2) \theta(\kappa^2 - Q_c^2). \quad (41)$$

Because the accepted propagation radius $R_c \sim 0.3$ fm for perturbative gluons is short compared to a typical range of strong interaction, the dipole cross section (35) evaluated with the DGSF (41) would miss an interaction strength in the soft region, for large color dipoles.

In Ref.[16, 17] interaction of large dipoles has been modeled by the non-perturbative, soft mechanism with energy-independent dipole cross section, whose specific form [16, 8] has been driven by early analysis [19] of the exchange by two nonperturbative gluons. More recently several closely related models for $\sigma_{soft}(r)$ have appeared in the literature, see for instance models for dipole-dipole scattering via polarization of non-perturbative QCD vacuum [29] and the model of soft-hard two-component pomeron [30]. In order to reproduce the required interaction strength for large dipoles, we introduce the genuinely soft, nonperturbative component of DGSF which we parameterize as

$$\mathcal{F}_{soft}^{(B)}(x, \kappa^2) = a_{soft} C_F N_c \frac{\alpha_s(\kappa^2)}{\pi} \left(\frac{\kappa^2}{\kappa^2 + \mu_{soft}^2}\right)^2 V_N(\kappa). \quad (42)$$

The principal point about this non-perturbative component of DGSF is that it must not be subjected to pQCD evolution. Thus the arguments about the hard-to-soft diffusion driven rise of perturbative DGSF even at small κ^2 do not apply to the non-perturbative DGSF and we take it energy-independent one. Such a nonperturbative component of DGSF would have certain high- κ^2 tail which should not extend too far. The desired suppression of soft DGSF at large- κ^2 and of hard DGSF (41) at moderate and small κ^2 can be achieved by the extrapolation of the form suggested in [5, 6]

$$\mathcal{F}(x, \kappa^2) = \mathcal{F}_{soft}^{(B)}(x, \kappa^2) \frac{\kappa_s^2}{\kappa^2 + \kappa_s^2} + \mathcal{F}_{hard}(x, \kappa^2) \frac{\kappa^2}{\kappa^2 + \kappa_h^2} \quad (43)$$

The above described Ansatz for DGSF must be regarded as a poor man's approximation. The separation of small- κ^2 DGSF into the genuine nonperturbative component and small- κ^2 tail

of the hard perturbative DGSF is not unique. Specifically, we attributed to the latter the same small- x rise as in the DGLAP fits at Q_c^2 while one can not exclude that the hard DGSF has a small x -independent component. The issue of soft-hard separation must be addressed in dynamical models for infrared regularization of perturbative QCD. As we shall see below, in section 4.4, the soft component of the above described Ansatz is about twice larger than the soft component used in the early color dipole phenomenology [16, 17].

The κ -factorization formulas (15) and (16) correspond to the full-phase space extension of the LO DGLAP approach at small x . For this reason our Ansätze for $\mathcal{F}_{hard}(x, Q^2)$ will be based on LO DGLAP fits to the gluon structure function of the proton $G_{pt}(x, Q^2)$. We consider the GRV98LO [10], CTEQ4L, version 4.6 [11] and MRS LO 1998 [12] parameterizations. We take the liberty of referring to our Ansätze for DGSF based on those LO DGLAP input as D-GRV, D-CTEQ and D-MRS parameterizations, respectively.

Our formulas (13), (14) describe the sea component of the proton structure function. Arguably these $LL\frac{1}{x}$ formulas are applicable at $x \lesssim x_0 = 1 \div 3 \cdot 10^{-2}$. At large Q^2 the experimentally attainable values of x are not so small. In order to give a crude idea on finite-energy effects at moderately small x , we stretch our fits to $x \gtrsim x_0$ multiplying the above Ansatz for DGSF by the purely phenomenological factor $(1-x)^5$ motivated by the familiar large- x behaviour of DGLAP parameterizations of the gluon structure function of the proton. We also add to the sea components (13), (14) the contribution from DIS on valence quarks borrowing the parameterizations from the respective GRV, CTEQ and MRS fits. The latter are only available for $Q^2 \geq Q_c^2$. At $x \lesssim 10^{-2}$ this valence contribution is small and fades away rapidly with decreasing x , for instance see [17].

5 Determination of the differential gluon structure function of the proton

5.1 The parameters of DGFS for different DGLAP inputs

Our goal is a determination of small- x DGSF in the whole range of κ^2 by adjusting the relevant parameters to the experimental data on small- x $F_{2p}(x, Q^2)$ in the whole available region of Q^2 as well as the real photoabsorption cross section. The theoretical calculation of these observables is based on Eqs. (15), (16), (43).

The parameters which we did not try adjusting but borrowed from early work in the color dipole picture are $R_c = 0.27$ fm, i.e., $\mu_{pt} = 0.75$ GeV and the frozen value of the LO QCD coupling with $\Lambda_{QCD} = 0.2$ GeV:

$$\alpha_S(Q^2) = \min \left\{ 0.82, \frac{4\pi}{\beta_0 \log \frac{Q^2}{\Lambda_{QCD}^2}} \right\}. \quad (44)$$

We recall that the GRV, MRS and CTEQ fits to GSF start the DGLAP evolution at quite a different soft-to-hard interface Q_c^2 and diverge quite a lot, especially at moderate and small κ^2 . The value of Q_c^2 is borrowed from these fits and is not a free parameter.

The adjustable parameters are μ_{soft} , a_{soft} , $m_{u,d}$, κ_s^2 and κ_h^2 . We take $m_s = m_{u,d} + 0.15$ GeV and $m_c = 1.5$ GeV. The rôle of these parameters is as follows. The quark mass $m_{u,d}$ defines the transverse size of the $q\bar{q} = u\bar{u}, d\bar{d}$ Fock state of the photon, whereas μ_{soft}^{-2} controls the

r -dependence of, and in conjunction with a_{soft} sets the scale for, the dipole cross section for large size $q\bar{q}$ dipoles in the photon. The both $m_{u,d}$ and μ_{soft} have clear physical meaning and we have certain insight into their variation range from the early work on color dipole phenomenology of DIS. The magnitude of the dipole cross section at large and moderately small dipole size depends also on the soft-to-hard interpolation of DGSF, which is somewhat different for different LO DGLAP inputs for $G_{pt}(x, Q^2)$. This difference of DGLAP inputs can be corrected for by adjusting μ_{soft}^2 and the value of κ_h^2 . Because of soft-to-hard and hard-to-soft diffusion the DGLAP fits are expected to fail at small x , we allow for x dependence of κ_h^2 .

Evidently, roughly equal values of $F_{2p}(x, Q^2)$ can be obtained for somewhat smaller $\mathcal{F}(x, Q^2)$ at the expense of taking smaller $m_{u,d}$ and vice versa. Therefore, though the quark mass does not explicitly enter the parameterization for $\mathcal{F}(x, \kappa^2)$, the preferred value of $m_{u,d}$ turns out to be correlated with the Ansatz for DGSF, i.e. each particular parameterization of DGSF implies certain $m_{u,d}$. In what follows we set $a_{soft} = 2$, $\kappa_s^2 = 3.0 \text{ GeV}^2$, $m_{u,d} = 0.22 \text{ GeV}$, so that only κ_h^2 and μ_{soft} varied from one DGLAP input to another, see Table 1. The soft components of the D-GRV and D-CTEQ parameterizations turn out identical. The eye-ball fits are sufficient for the purposes of the present exploratory study. The parameters found are similar to those used in [5, 6] where the focus has been on the description of diffractive DIS.

Table 1. The parameters of differential gluon structure function for different DGLAP inputs.

	D-GRV	D-MRS	D-CTEQ
LO DGLAP input	GRV98LO [10]	CTEQ4L(v.4.6) [11]	MRS-LO-1998 [12]
$Q_c^2, \text{ GeV}^2$	0.895	1.37	3.26
$\kappa_h^2, \text{ GeV}^2$	$(1 + 0.0018 \log^4 \frac{1}{x})^{1/2}$	$(1 + 0.038 \log^2 \frac{1}{x})^{1/2}$	$(1 + 0.047 \log^2 \frac{1}{x})^{1/2}$
$\mu_{soft}, \text{ GeV}$	0.1	0.07	0.1

One minor problem encountered in numerical differentiation of all three parameterizations for $G_{pt}(x, Q^2)$ was the seesaw κ^2 -behavior of the resulting DGSF (37), which was an artifact of the grid interpolation routines. Although this seesaw behavior of DGSF is smoothed out in integral observables like $G(x, Q^2)$ or $F_{2p}(x, Q^2)$, we still preferred to remove the unphysical seesaw cusps and have smooth DGSF. This was achieved by calculation DGSF from (37) at the center of each interval of the Q^2 -grid and further interpolation of the results between these points. By integration of the so-smoothed $\mathcal{F}_{pt}(x, Q^2)$ one recovers the input $G_{pt}(x, Q^2)$. The values of Q_c^2 cited in Table 1 corresponds to centers of the first bin of the corresponding Q^2 -grid.

5.2 The description of the proton structure function $F_{2p}(x, Q^2)$

We focus on the sea dominated leading $\log \frac{1}{x}$ region of $x < 10^{-2}$. The practical calculation of the proton structure function involves the two running arguments of DGSF: x_g and κ^2 . We recall that in the standard collinear DGLAP approximation one has $\kappa^2 \ll k^2 \ll Q^2$ and $x_g \approx 2x$, see eq. (23). Within the κ -factorization one finds that the dominant contribution to $F_{2p}(x, Q^2)$ comes from $M_t^2 \sim Q^2$ with little contribution from $M_t^2 \gtrsim Q^2$. Because at small x_g the x_g dependence of $\mathcal{F}(x_g, Q^2)$ is rather steep, we take into account the $x_g - x_{bj}$ relationship (19). Anticipating the results on effective intercepts to be reported in section 7, we notice

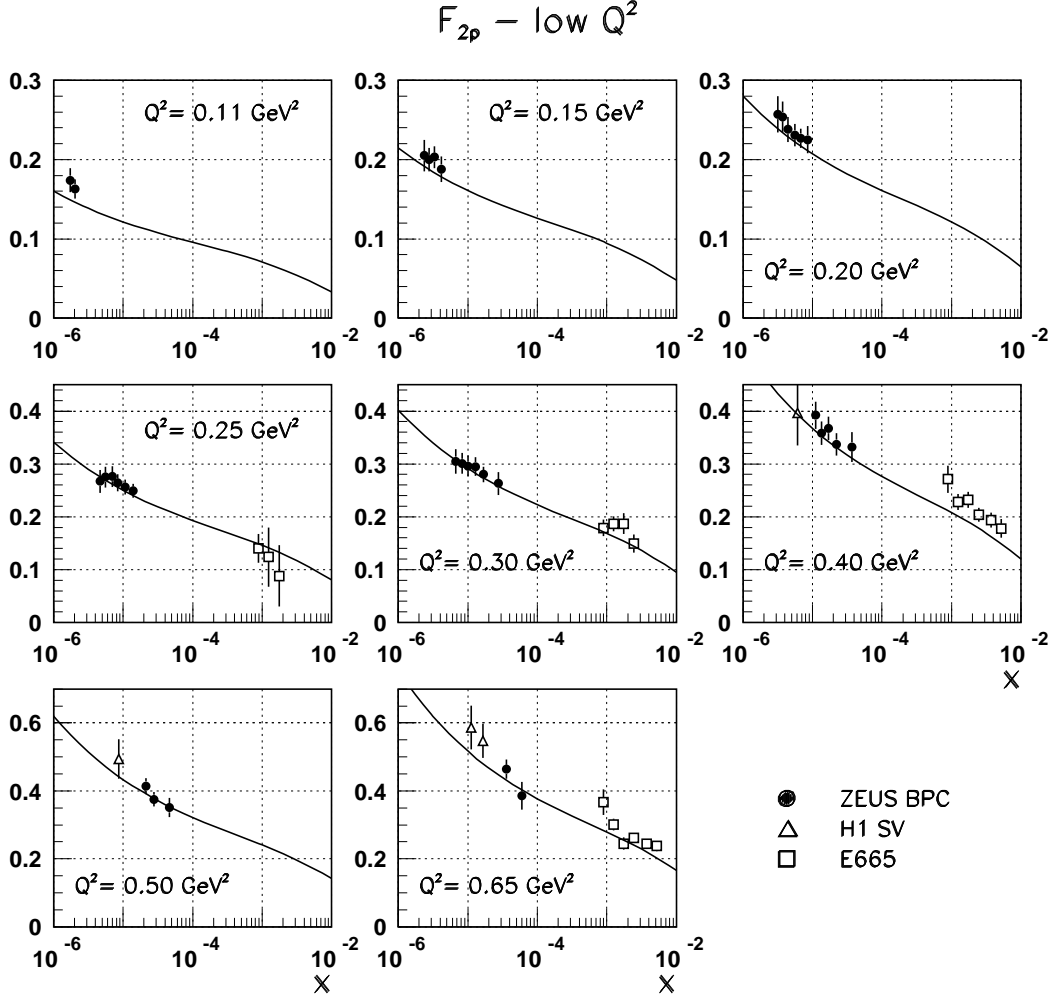


Figure 6: The κ -factorization description of the experimental data on $F_{2p}(x, Q^2)$ in the low Q^2 region; black circles are ZEUS BPC data [33], open triangles denote H1 shifted vertex (SV) data [35], open squares are E665 data [36]. Solid line represents κ -factorization results for the D-GRV parameterization of the differential gluon structure function $\mathcal{F}(x, \kappa^2)$.

that for all practical purposes one can neglect the impact of κ on the relationship (19), which simplifies greatly the numerical analysis. Indeed, the x_g dependence of $\mathcal{F}(x_g, \kappa^2)$ is important only at large κ^2 , which contribute to $F_{2p}(x, Q^2)$ only at large Q^2 ; but the larger Q^2 , the better holds the DGLAP ordering $\kappa^2 \ll k^2, Q^2$. Although at small to moderate Q^2 the DGLAP ordering breaks down, the x_g dependence of $\mathcal{F}(x_g, \kappa^2)$ is negligible weak here.

As we shall discuss in more detail below, achieving a good agreement from small to moderate to large Q^2 is a highly nontrivial task, because strong modification of the soft contribution to $\mathcal{F}(x, Q^2)$ unavoidably echos in the integral quantity $G_D(x, Q^2)$ throughout the whole range

F_{2p} – moderate and high Q^2

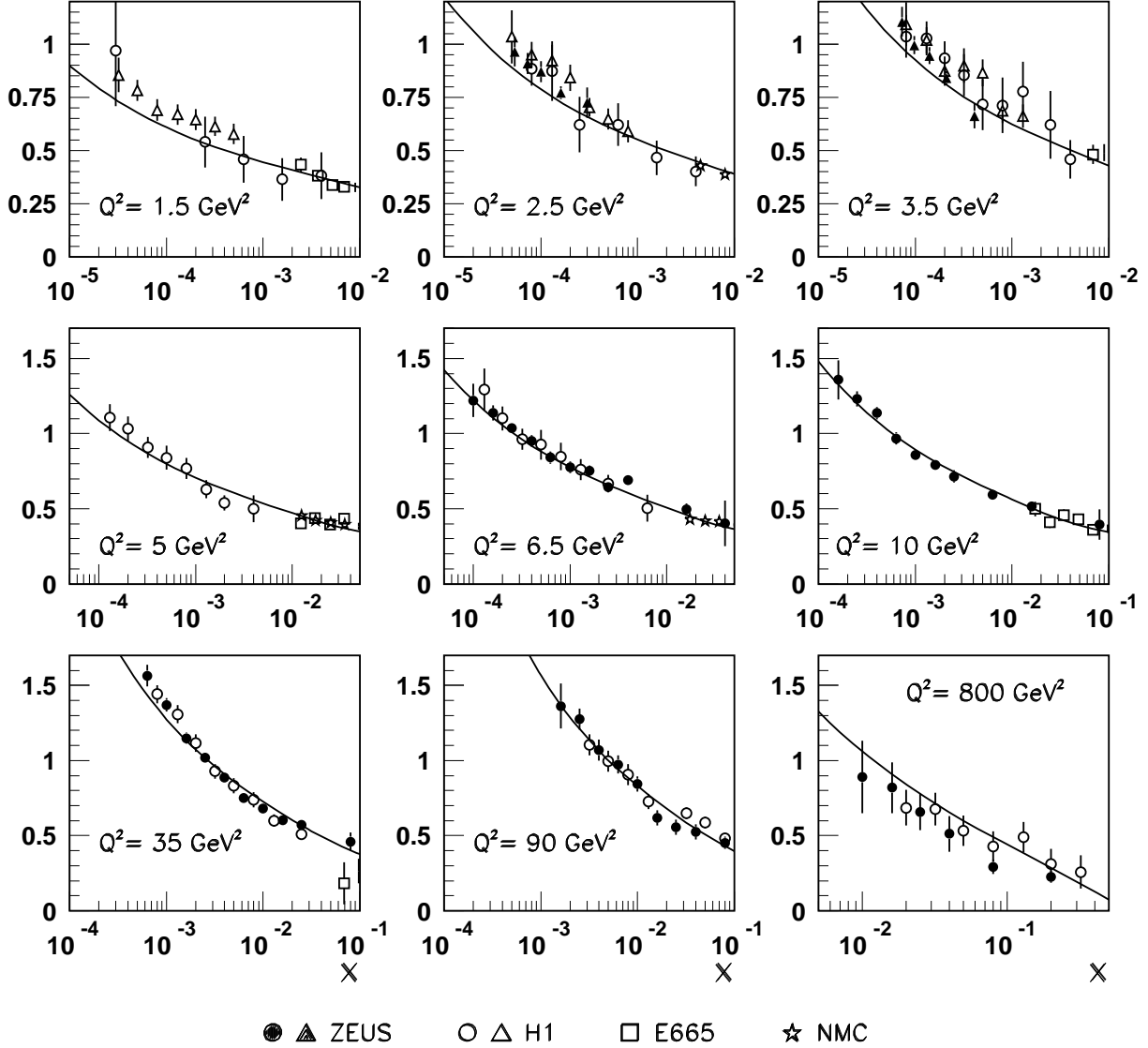


Figure 7: The κ -factorization description of the experimental data on $F_{2p}(x, Q^2)$ in the moderate and high Q^2 region; black circles and triangles are ZEUS data [31], [32], open circles and triangles show H1 data [34], [35], open squares are E665 data [36], stars refer to NMC results [37]. Solid line represents κ -factorization results for the D-GRV parameterization of the differential gluon structure function $\mathcal{F}(x, \kappa^2)$.

of Q^2 and shall affect the calculated structure function from small to moderate to large Q^2 .

The quality of achieved description of the experimental data on the small- x proton structure function is illustrated by figs. 6, 7. The data shown include recent HERA data (ZEUS [31], ZEUS shifted vertex [32], ZEUS BPC [33], H1 [34], H1 shifted vertex [35]), FNAL E665 experiment [36] and CERN NMC experiment [37]. When plotting the E665 and NMC data, we took the liberty of shifting the data points from the reported values of Q^2 to the closest Q^2 boxes for which the HERA data are available. For $Q^2 < Q_c^2 = 0.9 \text{ GeV}^2$ the parameterizations

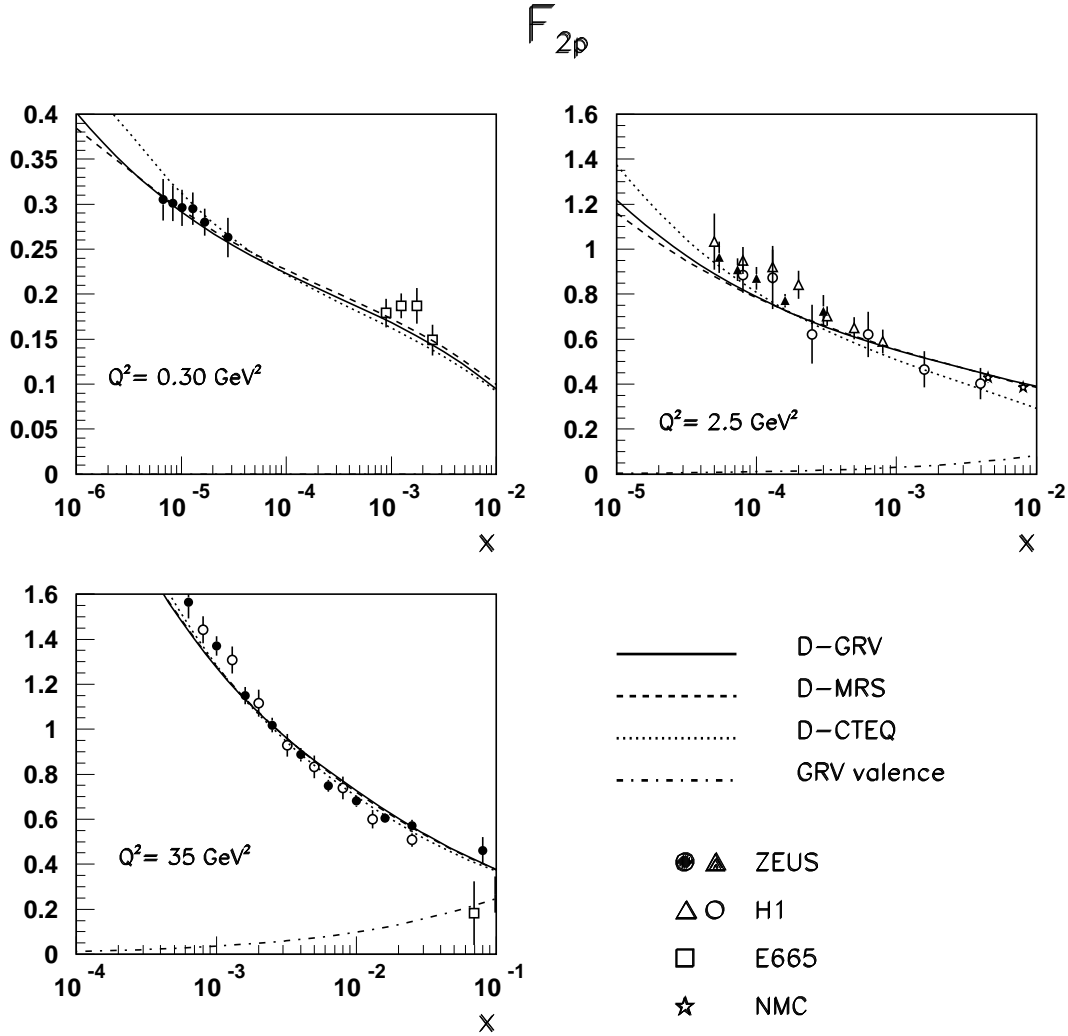


Figure 8: A comparison of the κ -factorization description of the experimental data on $F_{2p}(x, Q^2)$ for several values of Q^2 with the D-GRV, D-CTEQ and D-MRS parameterizations of the differential gluon structure function $\mathcal{F}(x, \kappa^2)$. The contribution to $F_{2p}(x, Q^2)$ from DIS off valence quarks is shown separately for larger Q^2 .

for valence distributions are not available and our curves show only the sea component of $F_{2p}(x, Q^2)$, at larger Q^2 the valence component is included.

At $x < 10^{-2}$ the accuracy of our D-GRV description of the proton structure function is commensurate to that of the accuracy of standard LO GRV fits. In order not to cram the figures with nearly overlapping curves, we show the results for D-GRV parameterization. The situation with D-CTEQ and D-MRS is very similar, which is seen in fig. 8, where we show on a larger scale simultaneously the results from the D-GRV, D-CTEQ and D-MRS DGSFs for several selected values of Q^2 . Here at large Q^2 we show separately the contribution from valence quarks. The difference between the results for $F_{2p}(x, Q^2)$ for different DGLAP inputs is marginal for all the practical purposes, see also a comparison of the results for $\sigma^{\gamma p}$ for different DGLAP inputs in fig. 9.

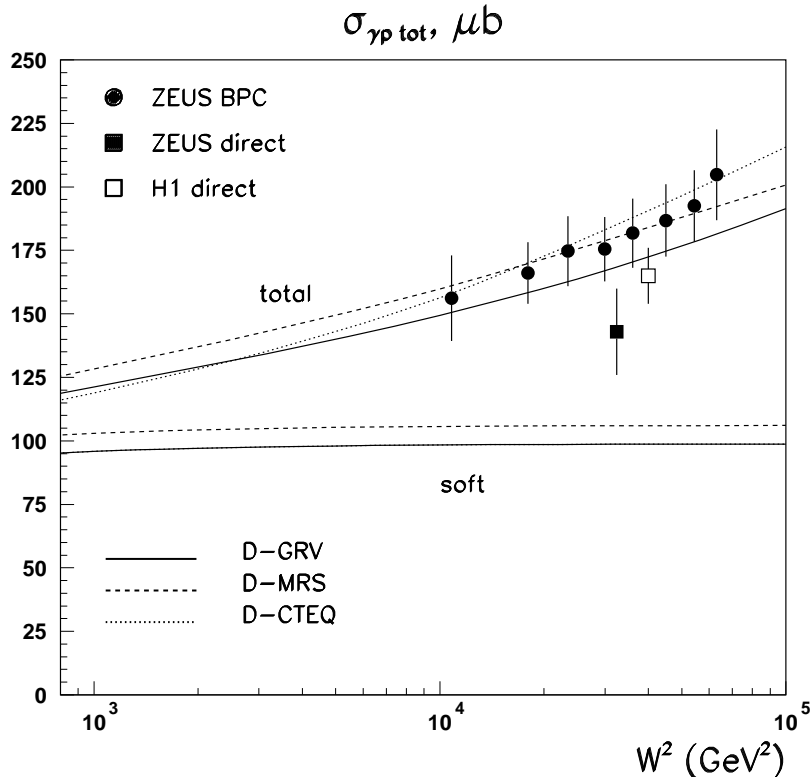


Figure 9: A comparison of the κ -factorization description of the experimental data on real photoabsorption cross section based on the D-GRV, D-CTEQ and D-MRS parameterizations of the differential gluon structure function $\mathcal{F}(x, \kappa^2)$. The squares show the experimental data from 1992-93 direct measurements, the bullets are the results of extrapolation of virtual photoabsorption to $Q^2 = 0$ ([33] and references therein). The soft component of photoabsorption cross section is shown separately.

5.3 Real photoabsorption cross section $\sigma^{\gamma p}$.

In the limiting case of $Q^2 = 0$ the relevant observable is the real photoabsorption cross section $\sigma^{\gamma p}$. Although the Bjorken variable is meaningless at very small Q^2 , the gluon variable x_g remains well defined at $Q^2 = 0$, see eq. (19). In fig. 9 we present our results alongside with the results of the direct measurements of $\sigma^{\gamma p}$ and the results of extrapolation of virtual photoabsorption cross sections to $Q^2 = 0$, for the summary of the experimental data see [33]. We emphasize that we reproduce well the observed magnitude and pattern of the energy dependence of $\sigma^{\gamma p}$ in an approach with the manifestly energy-independent soft contribution to the total cross section (which is shown separately in fig. 9). We recall that our parameterizations for $\mathcal{F}(x, Q^2)$ give identical soft cross sections for the GRV and CTEQ inputs (see table 1). The barely visible decrease of $\sigma_{soft}^{\gamma p}$ towards small W is a manifestation of $\propto (1-x)^5$ large- x behaviour of gluon densities. The extension to lower energies requires introduction of the secondary reggeon exchanges which goes beyond the subject of this study.

In our scenario the energy dependence of $\sigma^{\gamma p}$ is entirely due to the x_g -dependent hard component $\mathcal{F}_{hard}(x_g, Q^2)$ and as such this rise of the total cross section for soft reaction can be regarded as driven entirely by very substantial hard-to-soft diffusion. Such a scenario has repeatedly been discussed earlier [16, 17, 27]. Time and time again we shall see similar effects of hard-to-soft diffusion and vice versa. Notice that hard-to-soft diffusion is a straightforward consequence of full phase space calculation of partonic cross sections and we do not see any possibility for decoupling of hard gluon contribution from the total cross sections of any soft interaction, whose generic example is the real photoabsorption.

6 Properties of differential gluon structure function in the momentum space

6.1 Soft/hard decomposition of DGSF

Now we focus on the x and κ^2 behavior of the so-determined DGSF starting for the reference with the D-GRV parameterization. The same pattern holds for DGSF based on CTEQ and MRS DGLAP inputs, see below. In figs. 10 and 11 we plot the differential gluon density $\mathcal{F}(x_g, Q^2)$, while in fig. 12 we show the integrated gluon density

$$G_D(x, Q^2) = \int_0^{Q^2} \frac{d\kappa^2}{\kappa^2} \mathcal{F}(x, \kappa^2). \quad (45)$$

Here the subscript D is a reminder that the integrated $G_D(x, Q^2)$ is derived from DGSF. As such it must not be confused with the DGLAP parameterizations $G_{pt}(x, Q^2)$ supplied with the subscript pt .

Figs. 10 and 11 illustrate the interplay of the nonperturbative soft component of DGSF and perturbative hard contribution supplemented with the above described continuation into $\kappa^2 \leq Q_c^2$ at various x and κ^2 . The soft and hard contributions are shown by dashed and dotted lines respectively; their sum is given by solid line.

Apart from the large- x suppression factor $(1-x)^5$ our non-perturbative soft component does not depend on x . At a not so small $x = 10^{-2}$ it dominates the soft region of $\kappa^2 \lesssim 1 \div 2 \text{ GeV}^2$, the hard component takes over at higher κ^2 . The soft-hard crossover point is close to μ_{pt}^2 but because of the hard-to-soft diffusion it moves with decreasing x to a gradually smaller Q^2 .

6.2 Soft/hard decomposition of the integrated gluon structure function

The rôle of the soft component is further illustrated by fig. 12 where we show the integrated gluon density (45) and its soft and hard components $G_{soft}(x, Q^2)$ and $G_{hard}(x, Q^2)$, respectively. The soft contribution $G_{soft}(x, Q^2)$ is a dominant feature of the integrated gluon density $G_D(x, Q^2)$ for $Q^2 \lesssim 1 \text{ GeV}^2$. It builds up rapidly with Q^2 and receives the major contribution from the region $\kappa^2 \sim 0.3 \div 0.5 \text{ GeV}^2$. Our Ansatz for $\mathcal{F}_{soft}(x, \kappa^2)$ is such that it starts decreasing already at $\kappa^2 \sim 0.2 \text{ GeV}^2$ and vanishes rapidly beyond $\kappa^2 \gtrsim \kappa_{soft}^2$, see figs. 10,11. Still the residual rise of the soft gluon density beyond $Q^2 \sim 0.5 \text{ GeV}^2$ is substantial: $G_{soft}(x, Q^2)$ rises by about the factor two before it flattens at large Q^2 . We emphasize that $G_{soft}(Q^2)$ being

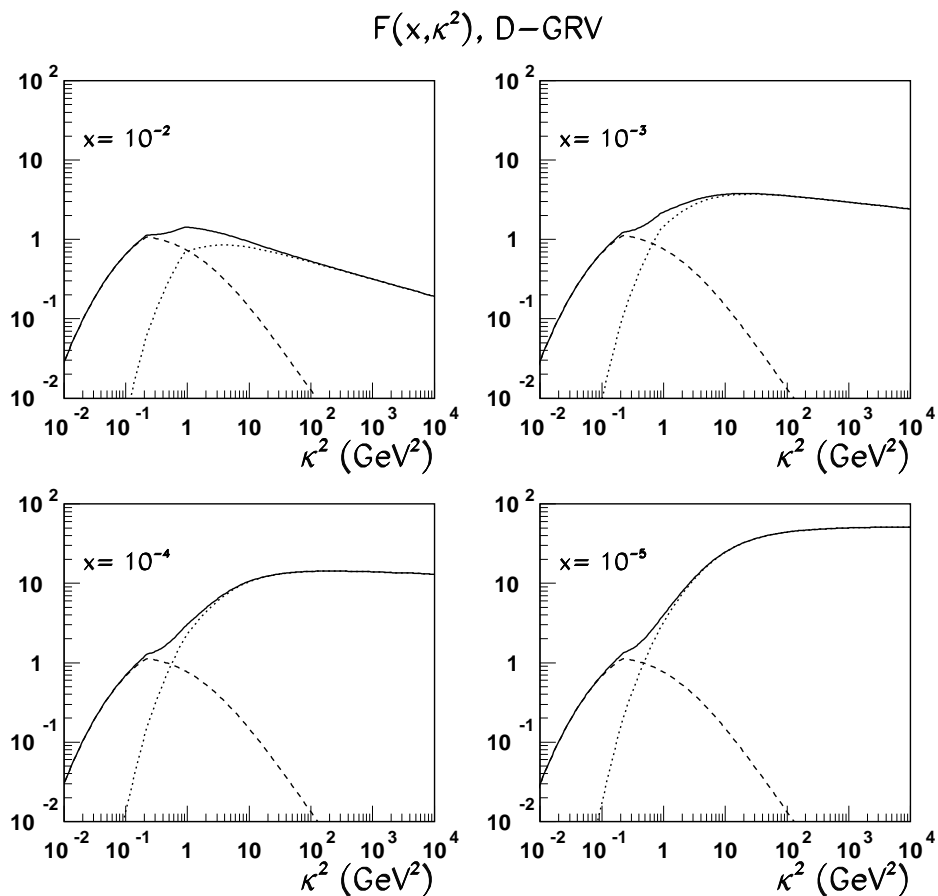


Figure 10: *D-GRV differential gluon structure function $\mathcal{F}(x, \kappa^2)$ as a function of κ^2 at several values of x . Dashed and dotted lines represent the soft and hard components; the total unintegrated gluon density is shown by the solid line*

finite at large Q^2 is quite natural — a decrease of $G_{soft}(Q^2)$ at large Q^2 only is possible if $\mathcal{F}_{soft}(Q^2)$ becomes negative valued at large Q^2 , which does not seem to be a viable option.

At moderately small $x = 10^{-2}$ the scaling violations are still weak and the soft contribution $G_{soft}(x, Q^2)$ remains a substantial part, about one half, of integrated GSF $G_D(x, Q^2)$ at all Q^2 . At very small $x \lesssim 10^{-3}$ the scaling violations in the gluon structure function are strong and $G_{hard}(x, Q^2) \gg G_{soft}(x, Q^2)$ starting from $Q^2 \sim 1-2 \text{ GeV}^2$.

6.3 Soft/hard decomposition of the proton structure function $F_2(x, Q^2)$

Eqs. (15), (16) define the soft/hard decomposition of the proton structure function. In fig. 13 we show $F_{2p}^{hard}(x, Q^2)$ and $F_{2p}^{soft}(x, Q^2)$ as a function of Q^2 for the two representative values of x . Notice how significance of soft component as a function of Q^2 rises from fully differential $\mathcal{F}(x, Q^2)$ to integrated $G_D(x, Q^2)$ to doubly integrated $F_{2p}^{soft}(x, Q^2)$. At a moderately small

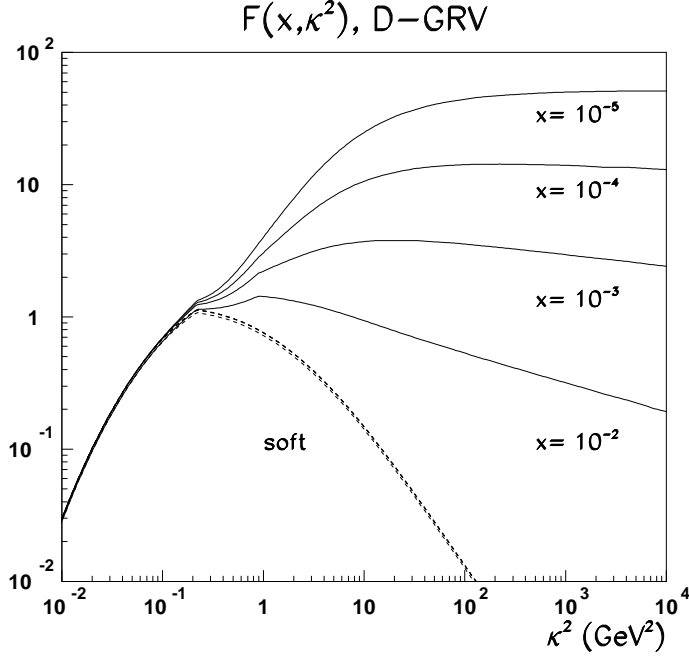


Figure 11: *The same as in Fig. 10 but overlaid onto one graph for illustration of the x -dependence of $\mathcal{F}(x, \kappa^2)$. The dashed lines shows the soft component $\mathcal{F}_{soft}(x, \kappa^2)$ and its slight variation with x due to the finite- x factor $(1-x)^5$.*

$x \sim 10^{-3}$ the soft contribution is a dominant part of $F_{2p}(x, Q^2)$, although the rapidly rising hard component $F_{2p}^{hard}(x, Q^2)$ gradually takes over at smaller x .

Notice that not only does $F_{2p}^{soft}(x, Q^2)$ not vanish at large Q^2 , but also it rises slowly with Q^2 as

$$F_{2p}^{soft}(x, Q^2) \sim \sum e_f^2 \frac{4G_{soft}(Q^2)}{3\beta_0} \log \frac{1}{\alpha_S(Q^2)}. \quad (46)$$

Again, the decrease of $F_{2p}^{soft}(x, Q^2)$ with Q^2 would only be possible at the expense of unphysical negative valued $G_{soft}(Q^2)$ at large Q^2 .

7 DGSF in the x -space: effective intercepts and hard-to-soft diffusion

It is instructive to look at the change of the x -dependence from the differential gluon structure function $\mathcal{F}(x, Q^2)$ to integrated gluon structure function $G_D(x, Q^2)$ to proton structure function $F_{2p}(x, Q^2)$. It is customary to parameterize the x dependence of various structure functions by the effective intercept. For instance, for the effective intercept τ_{eff} for differential gluon structure function is defined by the parameterization

$$\mathcal{F}(x, \kappa^2) \propto \left(\frac{1}{x}\right)^{\tau_{eff}(\kappa^2)}. \quad (47)$$

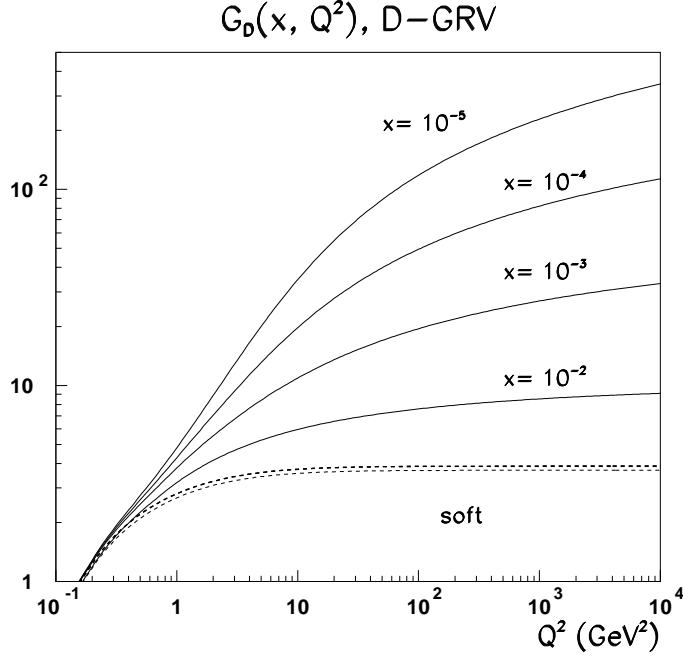


Figure 12: The same as Fig. 11 but for integrated gluon structure function $G_D(x, Q^2)$ as given by the D-GRV parameterization of the differential gluon structure function $\mathcal{F}(x, \kappa^2)$, for the discussion see Section 6.2.

One can define the related intercepts τ_{hard} for the hard component $\mathcal{F}_{hard}(x, Q^2)$. Notice, that in our Ansatz $\tau_{soft} \equiv 0$.

The power law (47) is only a crude approximation to the actual x dependence of DGSF and the effective intercept τ_{eff} will evidently depend on the range of fitted x . To be more definitive, for the purposes of the present discussion we define the effective intercept as

$$\tau_{eff}(Q^2) = \frac{\log[\mathcal{F}(x_2, \kappa^2)/\mathcal{F}(x_1, \kappa^2)]}{\log(x_1/x_2)} \quad (48)$$

taking $x_2 = 10^{-5}$ and $x_1 = 10^{-3}$. The effective intercept $\tau_{hard}(Q^2)$ is defined by (48) in terms of $\mathcal{F}_{hard}(x, Q^2)$.

One can define the related intercepts $\lambda_{eff}, \lambda_{hard}$ for the integrated gluon structure function $G_D(x, Q^2)$:

$$G_D(x, Q^2) \propto \left(\frac{1}{x}\right)^{\lambda_{eff}(Q^2)}. \quad (49)$$

In the case of $F_{2p}(x, Q^2)$ we define the intercept $\Delta(Q^2)$ in terms of the variable \bar{x} defined as

$$\bar{x} = \frac{Q^2 + M_V^2}{W^2 + Q^2} \sim x_g, \quad (50)$$

where M_V is the mass of the ground state vector meson in the considered flavor channel. Such a replacement allows one to treat on equal footing $Q^2 \lesssim 1 \text{ GeV}^2$, where the formally defined

F_{2p}, D-GRV

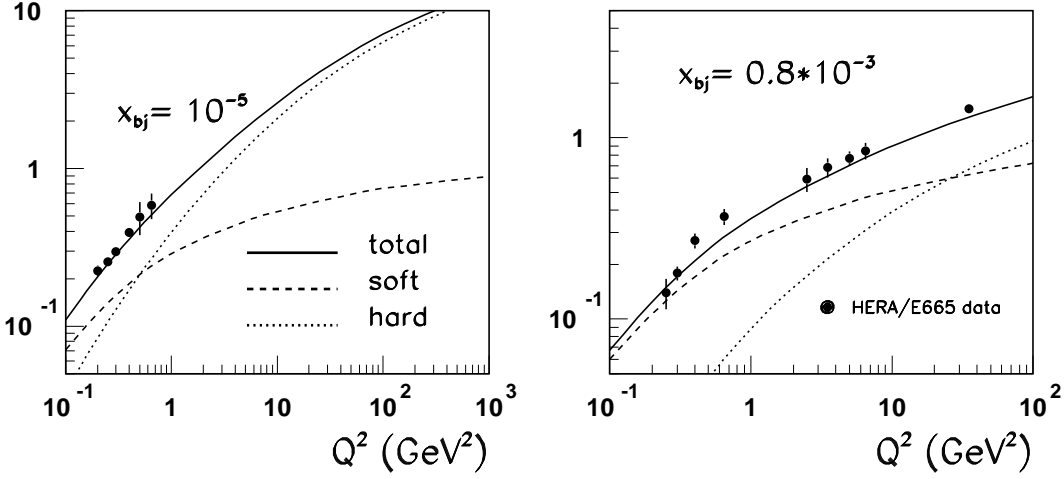


Figure 13: The soft-hard decomposition of κ -factorization results for the proton structure function $F_{2p}(x, Q^2)$ evaluated with the D-GRV parameterization of the differential gluon structure function $\mathcal{F}(x, \kappa^2)$.

Bjorken variable x_{bj} can no longer be interpreted as a lightcone momentum carried by charged partons. For the purposes of the direct comparison with $\tau(Q^2), \lambda(Q^2)$ and in order to avoid biases caused by the valence structure function, here we focus on intercepts $\Delta_{eff}, \Delta_{hard}$ for the sea component of the proton structure function $F_{2p}^{sea}(x, Q^2)$:

$$F_{2p}^{sea}(x, Q^2) \propto \left(\frac{1}{x}\right)^{\Delta_{eff}(Q^2)}. \quad (51)$$

The results for the effective intercepts are shown in figs. 14, 15 and 16.

In our simplified hard-to-soft extrapolation of $\mathcal{F}_{hard}(x, Q^2)$ we attribute to $\mathcal{F}_{hard}(x, Q^2)$ at $Q^2 \leq Q_c^2$ the same x -dependence as at $Q^2 = Q_c^2$ modulo to slight modifications for the x -dependence of κ_h^2 . This gives the cusp in $\tau_{hard}(Q^2)$ at $Q^2 = Q_c^2$, i.e., the first derivative of $\tau_{hard}(Q^2)$ is discontinuous at $Q^2 = Q_c^2$.

A comparison of fig. 11 with fig. 12 and further with fig. 13 shows clearly that only in DGSF $\mathcal{F}(x, Q^2)$ the effect of the soft component is concentrated at small Q^2 , in integrated $G_D(x, Q^2)$ and especially in the proton structure function $F_{2p}(x, Q^2)$ the impact of the soft component extends to much larger Q^2 . The larger the soft contribution, the stronger is the reduction of τ_{eff} from τ_{hard} and so forth, the pattern which is evident from fig. 14a to 14b to 14c, see also figs. 15 and 16.

The change of effective intercepts from differential $\mathcal{F}(x, Q^2)$ to integrated $G_D(x, Q^2)$ is straightforward, the principal effect is that $\lambda_{hard}(Q^2) < \tau_{hard}(Q^2)$ and $\lambda_{eff}(Q^2) < \tau_{eff}(Q^2)$ which reflects the growing importance of soft component in $G_D(x, Q^2)$. The change of effective intercepts from $\mathcal{F}(x, Q^2)$ and $G_D(x, Q^2)$ to $F_{2p}(x, Q^2)$ is less trivial and exhibits two dramatic

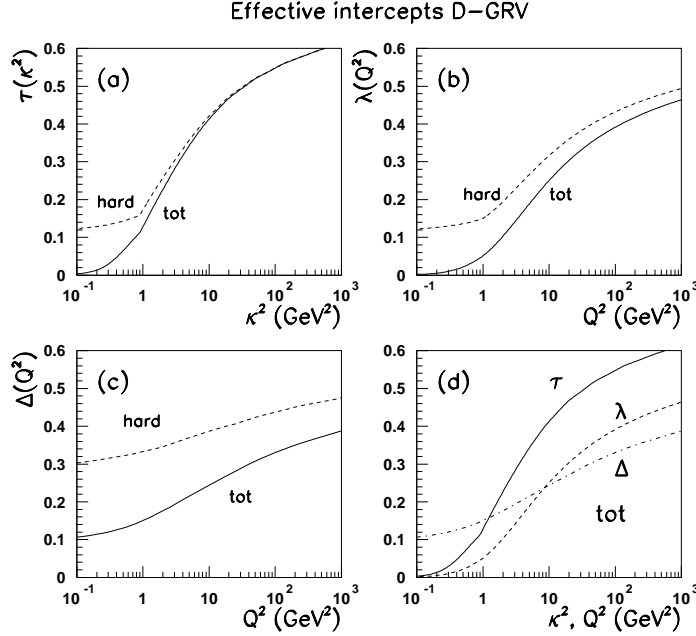


Figure 14: *Effective intercepts for total, and hard components of, (a) the differential gluon structure function $\mathcal{F}(x, Q^2)$; (b) integrated gluon structure function $G_D(x, Q^2)$ and (c) proton structure function $F_{2p}(x, Q^2)$ evaluated with the D-GRV parameterization of the differential gluon structure function $\mathcal{F}(x, \kappa^2)$. In the box (d) we compare the effective intercepts $\tau_{eff}(Q^2)$, $\lambda_{eff}(Q^2)$ and $\Delta_{eff}(Q^2)$ for $\mathcal{F}(x, Q^2)$, $G_D(x, Q^2)$ and $F_{2p}(x, Q^2)$, respectively.*

consequences of the hard-to-soft and soft-to-hard diffusion. If the standard DGLAP contribution (24) were all, then the change from the intercept $\lambda(Q^2)$ for integrated gluon density to the intercept $\Delta(Q^2)$ for the proton structure function $F_{2p}(x, Q^2)$ would have been similar to the change from $\tau(Q^2)$ to $\lambda(Q^2)$, i.e., the effective intercept $\Delta_{eff}(Q^2)$ would have been close to zero for $Q^2 \lesssim 1 \text{ GeV}^2$. However, by virtue of the hard-to-soft diffusion phenomenon inherent to the κ -factorization, $F_{2p}(x, Q^2)$ receives a contribution from gluons with $\kappa^2 > Q^2$, which enhances substantially $\Delta_{hard}(Q^2)$ and $\Delta_{eff}(Q^2)$. The net result is that at small to moderately large Q^2 we find $\Delta_{hard}(Q^2) > \lambda_{hard}(Q^2)$ and $\Delta_{eff}(Q^2) > \lambda_{eff}(Q^2)$. As we emphasized above in sections 5.3, the rise of real photoabsorption cross section is precisely of the same origin.

The second effect is a dramatic flattening of effective hard intercept, $\Delta_{hard}(Q^2)$, over the whole range of Q^2 . For all three DGLAP inputs $\Delta_{hard}(Q^2)$ flattens at approximately the same $\Delta_{hard} \approx 0.4$.

The whole set of figs. 14–16 also shows that the systematics of intercepts in the hard region of $Q^2 > Q_c^2$ is nearly identical for all the three DGLAP inputs. In the soft region we have a slight inequality $\tau_{hard}(\kappa^2)|_{D-MRS} > \tau_{hard}(\kappa^2)|_{D-GRV}$, which can be readily attributed to a slight inequality $Q_c^2(MRS) > Q_c^2(GRV)$. In the case of CTEQ4L(v.4.6) input the value of $Q_c^2(CTEQ)$ is substantially larger than $Q_c^2(MRS), Q_c^2(GRV)$. In the range $Q_c^2(MRS), Q_c^2(GRV) < \kappa^2 < Q_c^2(CTEQ)$ the effective intercept $\tau_{hard}(\kappa^2)$ rises steeply with κ^2 . This explains a why in the soft region $\tau_{hard}(\kappa^2)|_{CTEQ}$ is significantly larger than for the

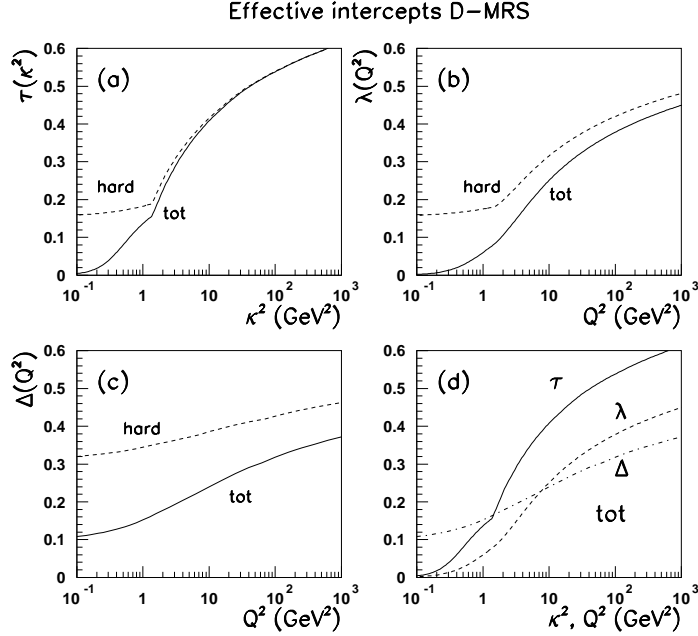


Figure 15: *Effective intercepts for total, and hard components of, (a) the differential gluon structure function $\mathcal{F}(x, Q^2)$; (b) integrated gluon structure function $G_D(x, Q^2)$ and (c) proton structure function $F_{2p}(x, Q^2)$ evaluated with the D-MRS parameterization of the differential gluon structure function $\mathcal{F}(x, \kappa^2)$. In the box (d) we compare the effective intercepts $\tau_{eff}(Q^2)$, $\lambda_{eff}(Q^2)$ and $\Delta_{eff}(Q^2)$ for $\mathcal{F}(x, Q^2)$, $G_D(x, Q^2)$ and $F_{2p}(x, Q^2)$, respectively.*

D-GRV and D-MRS parameterizations. The difference among intercepts for the three parameterizations decreases gradually from differential $\mathcal{F}(x, \kappa^2)$ to integrated $G_D(x, Q^2)$ gluon density to the proton structure function $F_{2p}(x, Q^2)$.

Finally, in fig. 17 we compare our results for $\Delta_{eff}(Q^2)$ with the recent experimental data from ZEUS collaboration [32]. In the experimental fit the range of $x = [x_{max}, x_{min}]$ varies from point to point, in our evaluation of Δ_{eff} from eq. (55) we mimicked the experimental procedure taking $\bar{x}_2 = x_{max}$ and $\bar{x}_1 = x_{min}$. This explains the somewhat irregular Q^2 dependence. The experimental data include both sea and valence components. At $Q^2 > Q_c^2(GRV) = 0.9$ GeV² we included the valence component of the structure function taking the GRV98LO parameterization. For CTEQ4L(v.4.6) and MRS-LO-1998 the values of Q_c^2 are substantially larger. However, the valence component is a small correction and we took a liberty of evaluating the valence contribution $F_{2p}^{val}(x, Q^2)$ for $Q_c^2(GRV) < Q^2 < Q_c^2(MRS), Q_c^2(CTEQ)$. The overall agreement with experiment is good. Difference among the three parameterization is marginal and can of course be traced back to figs. 14–16.

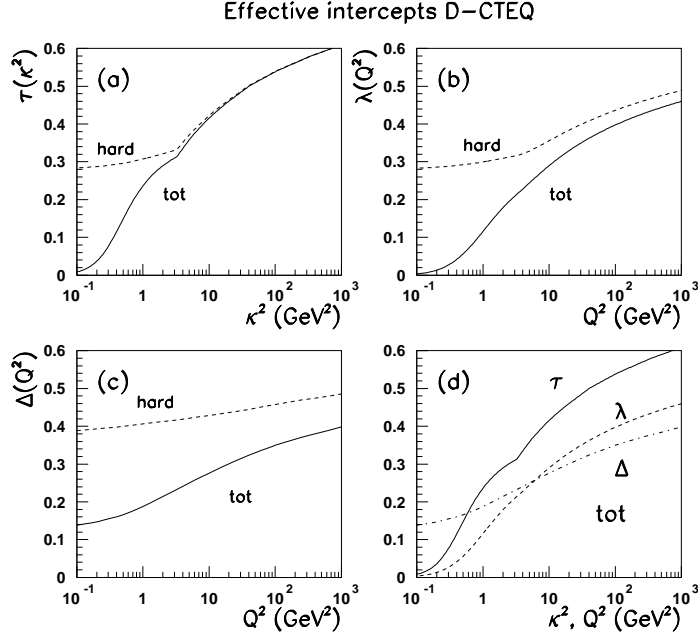


Figure 16: *Effective intercepts for total, and hard components of, (a) the differential gluon structure function $\mathcal{F}(x, Q^2)$; (b) integrated gluon structure function $G_D(x, Q^2)$ and (c) proton structure function $F_{2p}(x, Q^2)$ evaluated with the D-CTEQ parameterization of the differential gluon structure function $\mathcal{F}(x, \kappa^2)$. In the box (d) we compare the effective intercepts $\tau_{eff}(Q^2)$, $\lambda_{eff}(Q^2)$ and $\Delta_{eff}(Q^2)$ for $\mathcal{F}(x, Q^2)$, $G_D(x, Q^2)$ and $F_{2p}(x, Q^2)$, respectively.*

8 How the gluon densities of κ -factorization differ from DGLAP gluon densities

It is instructive also to compare our results for integrated GSF (45) with the conventional DGLAP fit $G_{pt}(x, Q^2)$. In fig. 18 we present such a comparison between our integrated D-GRV distribution (the solid curves) and the GRV98LO distribution (the dashed curves). As was anticipated in section 3.2, at very large Q^2 the two gluon distributions converge. We also anticipated that at small x and moderate Q^2 the DGLAP gluon structure functions $G_{pt}(x, Q^2)$ are substantially larger than the result of integration of DGSF, see eq. (45). At $x = 10^{-5}$ they differ by as much as the factor two-three over a broad range of $Q^2 \lesssim 100$ GeV². The difference between integrated DGSF and the DGLAP fit decreases gradually at large x , and is only marginal at $x = 10^{-2}$.

Recall the substantial divergence of the GRV, MRS and CTEQ gluons structure functions of DGLAP approximation $G_{pt}(x, Q^2)$ at small and moderate Q^2 . Contrary to that, the κ -factorization D-GRV, D-CTEQ and D-MRS gluon structure functions $G_D(x, Q^2)$ are nearly identical. We demonstrate this property in fig. 19 where we show integrated $G_D(x, Q^2)$ and their DGLAP counterparts $G_{pt}(x, Q^2)$ for the three parameterizations at two typical values of x . Because of an essentially unified treatment of the region of $\kappa^2 \leq Q_c^2$ and strong constraint on DGSF in this region from the experimental data at small Q^2 , such a convergence of D-GRV,

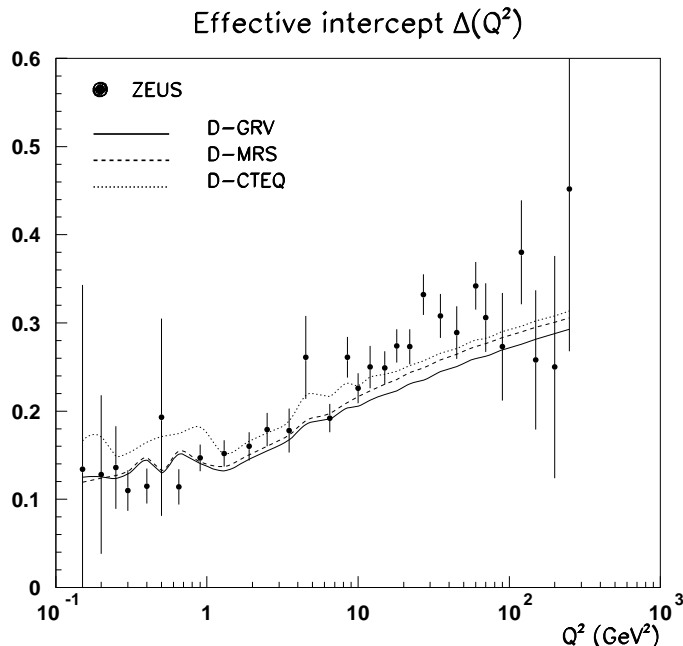


Figure 17: *Effective intercepts $\Delta(Q^2)$ of the proton structure function $F_{2p}(x, Q^2)$ in the HERA domain evaluated for the D-GRV, D-MRS and D-CTEQ parameterizations for the differential gluon structure function $\mathcal{F}(x, \kappa^2)$; the experimental data points are from ZEUS [32]*

D-CTEQ and D-MRS DGSF's is not unexpected.

One can also compare the effective intercepts for our integrated GSF $G_D(x, Q^2)$ with those obtained from DGLAP gluon distributions $G_{pt}(x, Q^2)$. Fig.20 shows large scattering of $\lambda_{eff}^{(pt)}(Q^2)$ from one DGLAP input to another. At the same time, this divergence of different DGLAP input parameterizations is washed out to a large extent in the κ -factorization description of physical observables (see also 17).

9 How different observables probe the DGSF $\mathcal{F}(x, Q^2)$

The issue we address in this section is how different observables map the κ^2 dependence of $\mathcal{F}(x_g, \kappa^2)$. We expand on the qualitative discussion in section 3.2 and corroborate it with numerical analysis following the discussion in [20]. We start with the two closely related quantities — longitudinal structure function $F_L(x, Q^2)$ and scaling violations $\partial F_2(x, Q^2)/\partial \log Q^2$ — and proceed to $F_{2p}(x, Q^2)$ and the charm structure function of the proton $F_{2p}^{c\bar{c}}(x, Q^2)$. This mapping is best studied if in (15) and (16) we integrate first over \mathbf{k} and z . In order to focus on the κ^2 dependence we prefer presenting different observables in terms of $\mathcal{F}(2x, \kappa^2)$ and $G_D(2x, \kappa^2)$

$$F_L(x, Q^2) = \frac{\alpha_S(Q^2)}{3\pi} \sum e_f^2 \int \frac{d\kappa^2}{\kappa^2} \Theta_L^{(f\bar{f})}(Q^2, \kappa^2) \mathcal{F}(2x, \kappa^2), \quad (52)$$

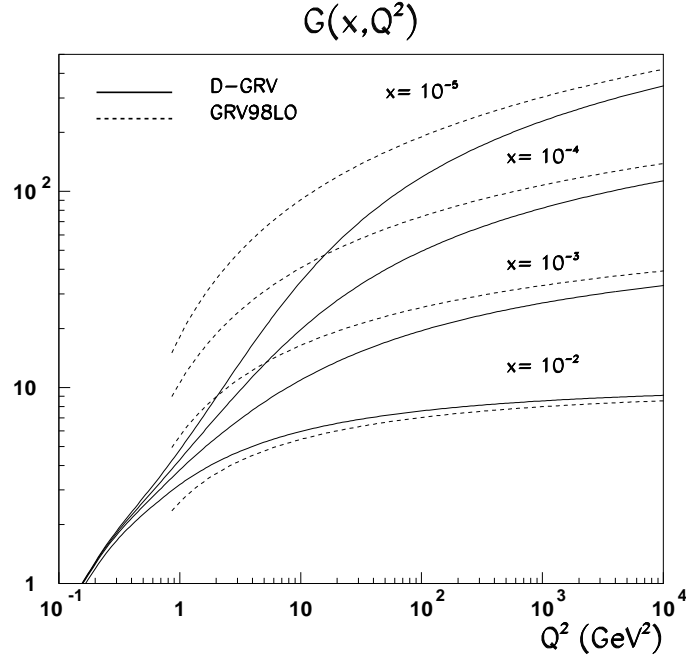


Figure 18: Comparison of our results for integrated gluon density $G_D(x, Q^2)$ evaluated with the D-GRV parameterization of the differential gluon structure function $\mathcal{F}(x, \kappa^2)$ with the GRV98LO DGLAP input parameterization $G_{pt}(x, Q^2)$.

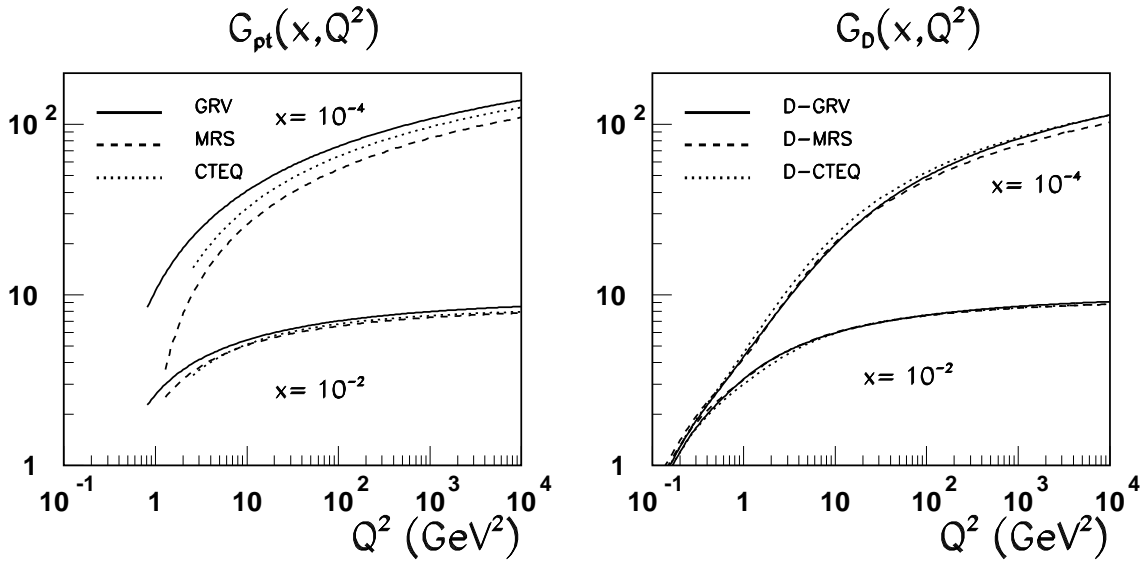


Figure 19: A comparison of the divergence of GRV98LO, CTEQ_{4L}(v.4.6) and MRS-LO-1998 gluon structure functions $G_{pt}(x, Q^2)$ in the left box with the divergence of our integrated gluon structure functions $G_D(x, Q^2)$ evaluated for the D-GRV, D-CTEQ and D-MRS parameterizations for differential gluon structure function $\mathcal{F}(x, Q^2)$ at two typical values of x

Effective intercepts $\lambda(Q^2)$

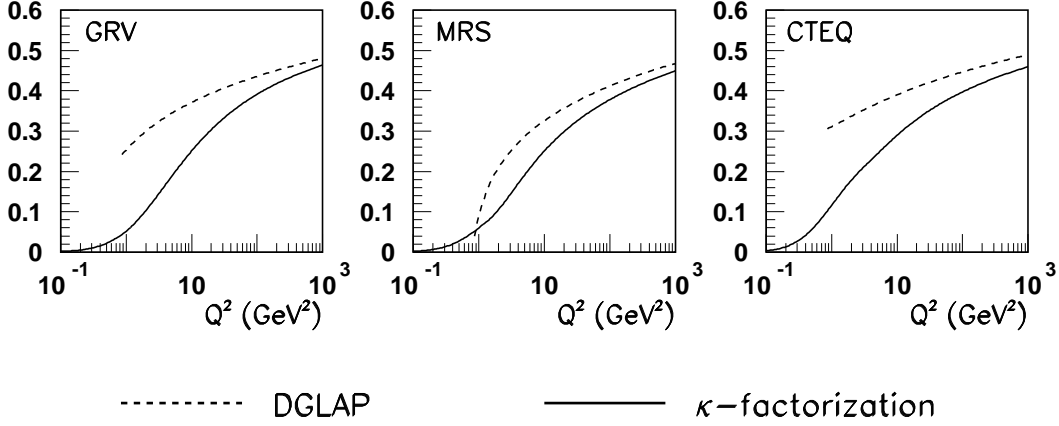


Figure 20: A comparison of the intercept $\lambda_{eff}^{(pt)}(Q^2)$ of the x -dependence of the GRV98L0, CTEQ4L(v.4.6) and MRS-LO-1998 gluon structure functions $G_{pt}(x, Q^2)$ with their counterpart $\lambda_{eff}(Q^2)$ for integrated $G_D(x, Q^2)$ evaluated with D-GRV, D-CTEQ and D-MRS parameterizations for differential gluon structure function $\mathcal{F}(x, Q^2)$.

$$\frac{\partial F_2(x, Q^2)}{\partial \log Q^2} = \frac{\alpha_S(Q^2)}{3\pi} \sum e_f^2 \int \frac{d\kappa^2}{\kappa^2} \Theta_2^{(f\bar{f})}(Q^2, \kappa^2) \mathcal{F}(2x, \kappa^2). \quad (53)$$

In the numerical calculation of $F_L(x, Q^2)$ starting from eq. (16) we have x_g and κ^2 as the two running arguments of $\mathcal{F}(x_g, \kappa^2)$. As discussed above, the mean value of x_g is close to $2x$, but the exact relationship depends on κ^2 . The \mathbf{k}, z integration amounts to averaging of $\mathcal{F}(x_g, \kappa^2)$ over certain range of x_g . The result of this averaging is for the most part controlled by the effective intercept $\tau_{eff}(\kappa^2)$:

$$\langle \mathcal{F}(x_g, \kappa^2) \rangle = \left\langle \mathcal{F}(2x, \kappa^2) \left(\frac{2x}{x_g} \right)^{\tau_{eff}(\kappa^2)} \right\rangle = r(\kappa^2) \mathcal{F}(2x, \kappa^2). \quad (54)$$

Because the derivative of $\tau_{eff}(\kappa^2)$ changes rapidly around $\kappa^2 = Q_c^2$, the rescaling factor $r(\kappa^2)$ also has a rapid variation of the derivative at $\kappa^2 = Q_c^2$, which in the due turn generates the rapid change of derivatives of $\Theta_{L,2}^{(f\bar{f})}(Q^2, \kappa^2)$ around $\kappa^2 = Q_c^2$. As far as the mapping of differential $\mathcal{F}(2x, \kappa^2)$ is concerned, this is an entirely marginal effect. However, if we look at the mapping of integrated gluon structure function $G_D(x, Q^2)$, which is derived from (52), (53) by integration by parts:

$$F_L(x, Q^2) = -\frac{\alpha_S(Q^2)}{3\pi} \sum e_f^2 \int \frac{d\kappa^2}{\kappa^2} \frac{\partial \Theta_L^{(f\bar{f})}(Q^2, \kappa^2)}{\partial \log \kappa^2} G_D(2x, \kappa^2), \quad (55)$$

$$\frac{\partial F_2(x, Q^2)}{\partial \log Q^2} = -\frac{\alpha_S(Q^2)}{3\pi} \sum e_f^2 \int \frac{d\kappa^2}{\kappa^2} \frac{\partial \Theta_2^{(f\bar{f})}(Q^2, \kappa^2)}{\partial \log \kappa^2} G_D(2x, \kappa^2), \quad (56)$$

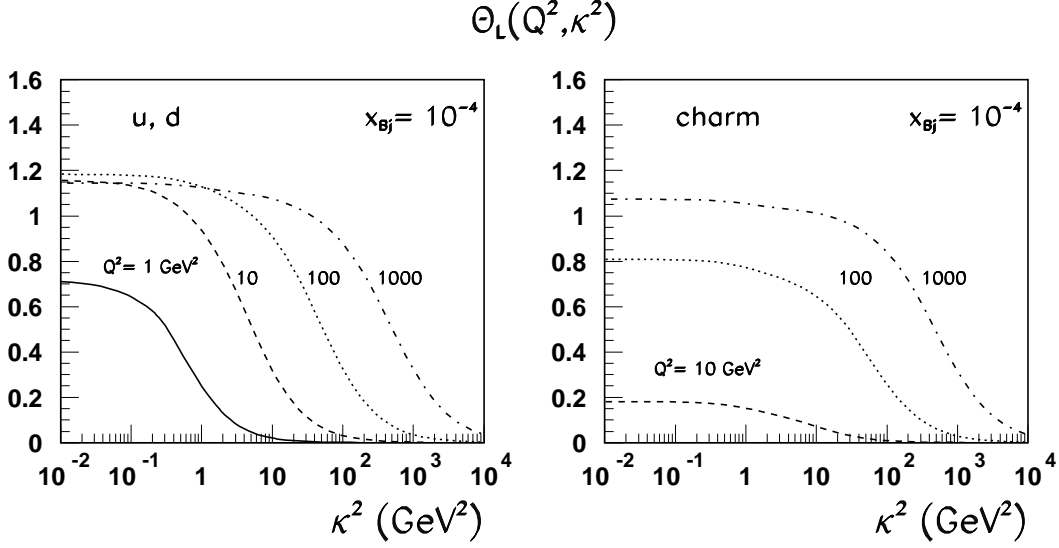


Figure 21: The weight function Θ_L for mapping of the differential gluon structure function $\mathcal{F}(x, \kappa^2)$ as a function of κ^2 for several values of Q^2 . We show separately the results for light flavours, u, d , and charm.

then the weight functions $\partial\Theta_{2,L}^{(f\bar{f})}(Q^2, \kappa^2)/\partial\log\kappa^2$ will exhibit a slightly irregular behaviour around $\kappa^2 = Q_c^2$. Evidently, such an irregularity appears in any region of fast variation of $\tau_{eff}(\kappa^2)$; in our simplified model it is somewhat amplified by the cusp-like κ^2 dependence of $\tau_{eff}(\kappa^2)$.

Finally, starting from (56) one obtains a useful representation for how the proton structure function $F_{2p}(x, Q^2)$ maps the integrated gluon structure function:

$$\begin{aligned}
 F_{2p}(x, Q^2) &= - \int_0^{Q^2} \frac{dq^2}{q^2} \frac{\alpha_S(q^2)}{3\pi} \sum e_f^2 \int \frac{d\kappa^2}{\kappa^2} \frac{\partial\Theta_2^{(f\bar{f})}(q^2, \kappa^2)}{\partial\log\kappa^2} G_D(2x, \kappa^2) \\
 &= \frac{1}{3\pi} \sum e_f^2 \int \frac{d\kappa^2}{\kappa^2} W_2^{(f\bar{f})}(Q^2, \kappa^2) \alpha_S(\kappa^2) G_D(2x, \kappa^2)
 \end{aligned} \tag{57}$$

In figs. 21 and 22 we show the weight functions Θ_L and Θ_2 . Evidently, for light flavours and very large Q^2 they can be approximated by step-functions

$$\Theta_{L,2}^{(f\bar{f})}(Q^2, k^2) \sim \theta(C_{L,2}Q^2 - \kappa^2), \tag{58}$$

where the scale factors $C_L \sim \frac{1}{2}$ and $C_2 \sim 2$ can be readily read from figures, for the related discussion see [20]. Note that the value $C_2 \sim 2$ corresponds to $\bar{C}_2 \sim 8$ introduced in Section 3.2. Recall that the development of the plateau-like behaviour of Θ_L and Θ_2 which extends to $\kappa^2 \sim Q^2$ signals the onset of the leading $\log Q^2$ approximation. For large Q^2 in the approximation (58) the κ^2 integration can be carried out explicitly and $F_L(x, Q^2) \propto G_D(2x, C_L Q^2)$. Similarly, $\partial F_2(x, Q^2)/\partial\log Q^2 \propto G_D(2x, C_2 Q^2)$, cf. eq. (28).

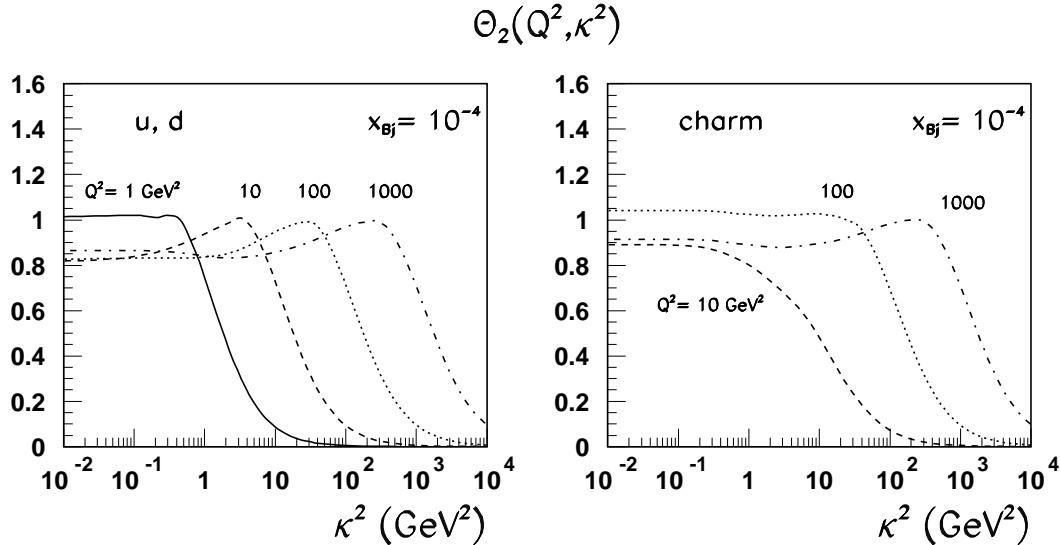


Figure 22: The weight function Θ_2 for mapping of the differential gluons structure function $\mathcal{F}(x, \kappa^2)$ as a function of κ^2 for several values of Q^2 . We show separately the results for light flavours, u, d , and charm.

Still better idea on how F_L and scaling violations map the integrated GSF is given by figs. 23,24, where we show results for $-\partial\Theta(ff)_L/\partial\log\kappa^2$ and $W_2^{(ff)}$. The first quantity is sharply peaked at $\kappa^2 \sim C_L Q^2$. The second quantity visibly develops a plateau at large Q^2 . As can be easily seen, scaling violations do receive a substantial contribution from the beyond-DGLAP region of $\kappa^2 > Q^2$.

Because of the heavy mass, the case of the charm structure function $F_{2p}^{c\bar{c}}(x, Q^2)$ is somewhat special. Figs. 23 and 24 show weak sensitivity of $F_{2p}^{c\bar{c}}(x, Q^2)$ to a soft component of $\mathcal{F}(x_{bj}, \kappa^2)$ which has an obvious origin: long-wavelength soft gluons with $\kappa \lesssim m_c$ decouple from the color neutral $c\bar{c}$ Fock state of the photon which has a small transverse size $\lesssim \frac{1}{m_c}$. Our results for $F_{2p}^{c\bar{c}}(x, Q^2)$ are shown in fig. 25, the agreement with the recent precision experimental data from ZEUS [38] is good.

10 Summary and outlook

We present the first parameterization of differential gluon structure function $\mathcal{F}(x, Q^2)$ of the proton inherent to the κ -factorization approach to small- x DIS. The form of the parameterization is driven by color gauge invariance constraints for soft Q^2 , early ideas from color dipole phenomenology on the necessity of nonperturbative soft mechanism for interaction of large color dipoles and by matching to the derivative of familiar DGLAP fits $G_{pt}(x, Q^2)$. The latter condition is not imperative, though, and can be relaxed; in this exploratory study we simply wanted to take advantage of the insight on $G_{pt}(x, Q^2)$ from early DGLAP approximation stud-

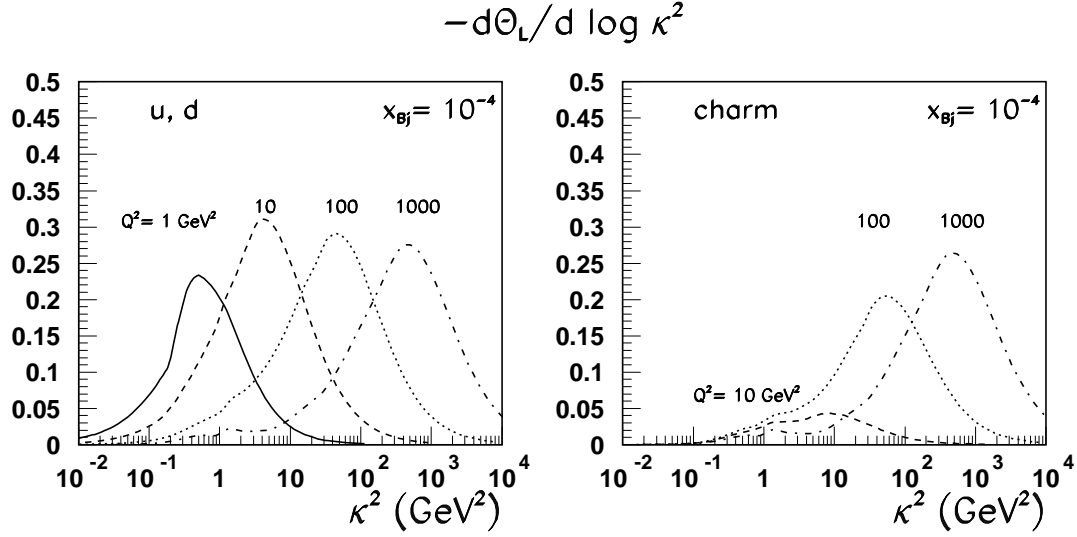


Figure 23: *The same as Fig. 21 but for mapping of the integrated gluon structure function $G_D(x, \kappa^2)$ as a function of κ^2 for several values of Q^2 . We show separately the results for light flavours and charm.*

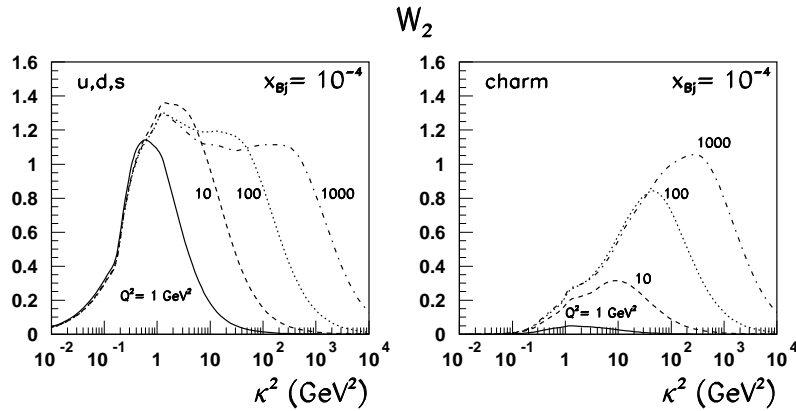


Figure 24: *The weight function W_2 for mapping of the integrated gluons structure function $G_D(x, \kappa^2)$ as a function of κ^2 for several values of Q^2 . We show separately the results for light flavours and charm*

ies on scaling violations. The parameters of $\mathcal{F}(x, Q^2)$ have been tuned to the experimental data on F_{2p} in the low- x ($x \lesssim 0.01$) domain and throughout the entire Q^2 region as well as on real photoabsorption cross section $\sigma_{tot}^{\gamma p}$. Differential gluon structure function $\mathcal{F}(x, Q^2)$ is the

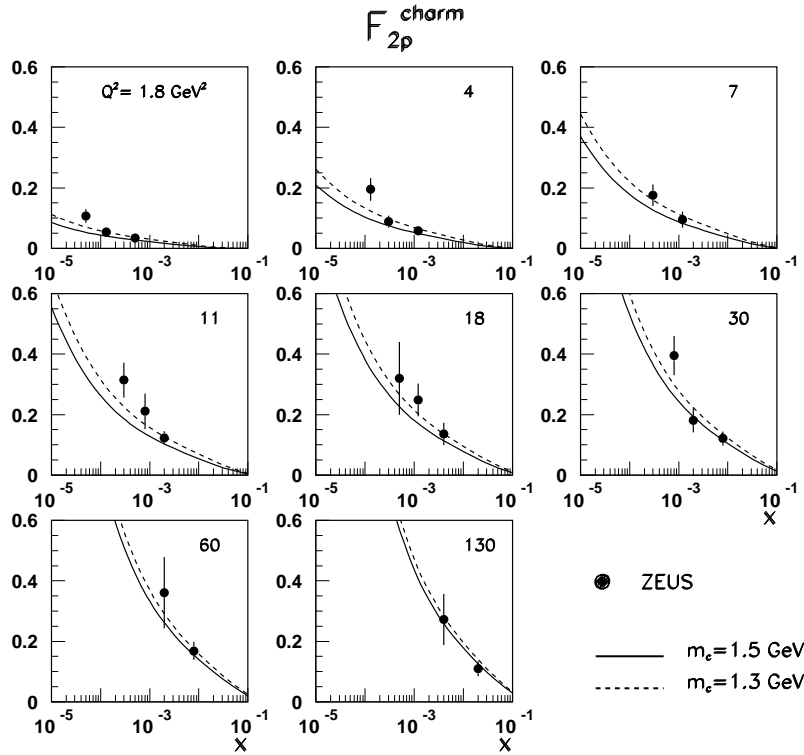


Figure 25: A comparison of the experimental data from ZEUS [38] on the charm structure function of the proton with κ -factorization results for $F_2^{c\bar{c}}(x, Q^2)$ based on the D-GRV parameterization of the differential gluon structure function $\mathcal{F}(x, Q^2)$.

principal input for pQCD calculation of many diffractive processes and we anticipate that the consistent use of our parameterizations shall reduce the uncertainties of calculations of cross section of such processes as diffractive DIS into vector mesons and continuum.

Our results allow to address several interesting issues. First, our Ansätze for $\mathcal{F}(x, Q^2)$ have been so constructed as to ensure the convergence of $G_D(x, Q^2)$ — the integral of $\mathcal{F}(x, Q^2)$ — to the corresponding large Q^2 DGLAP input $G_{pt}(x, Q^2)$. We notice that both gluon distributions provide a comparable description of the same set of the experimental data on the proton structure function, the only difference being that in the κ -factorization we lift the DGLAP limitation on the transverse phase space of quarks and antiquarks. We find very slow convergence of, and numerically very large difference between, the κ -factorization distribution $G_D(x, Q^2)$ and the DGLAP fit $G_{pt}(x, Q^2)$. As anticipated, the divergence of the two distributions is especially large at small- x and persists even in the hard region up to $Q^2 \sim 10 \div 100 \text{ GeV}^2$ at $x = 10^{-5}$. We interpret this divergence as a signal of breaking of the DGLAP approximation which arguably gets poorer at smaller x . The second finding is a numerically very strong impact of soft gluons on the integrated gluons structure function $G_D(x, Q^2)$ and the proton structure function $F_{2p}(x, Q^2)$. It is not unexpected in view of the early work on color dipole phenomenology of small- x DIS, but the evaluation of the soft component of integrated gluon

structure function is reported here for the first time. In conjunction with the strong departure of the κ -factorization distribution $G_D(x, Q^2)$ from the DGLAP fit $G_{pt}(x, Q^2)$ it serves as a warning against unwarranted application of DGLAP evolution at Q^2 in the range of several GeV^2 .

The phenomenologically most interesting finding is the anatomy of the rising component of the proton structure function from the Regge theory point of view. We notice that effective intercepts $\tau_{hard}(Q^2)$ and λ_{hard} for hard components of the differential and integrated gluon distributions are lively functions of Q^2 which vary quite rapidly with Q^2 from ≈ 0.1 at small Q^2 to ≈ 0.6 at $Q^2 \sim 10^3 \text{ GeV}^2$. In the Regge theory language this evidently implies that hard component of neither $\mathcal{F}(x, Q^2)$ nor $G_D(x, Q^2)$ is dominated by a single Regge pole exchange and a contribution from several hard Regge poles with broad spacing of intercepts is called upon. However, an approximately flat Q^2 dependence of $\Delta_{hard}(Q^2)$ shows that the hard component of the proton structure function can well be approximated by a single Regge pole with intercept $\Delta_{hard} \approx 0.4$. Such a scenario in which a contribution of subleading BFKL-Regge poles to $F_{2p}(x, Q^2)$ is suppressed dynamically because of the nodal properties of gluon distributions for subleading BFKL-Regge poles has been encountered earlier in the color dipole BFKL approach [17]. The intercept $\Delta_{hard}(Q^2)$ found in the present analysis is remarkably close the intercept of the leading BFKL-Regge pole $\Delta_{\mathbf{P}} = 0.4$ found in the color dipole approach in 1994 [16, 17, 21]. For the related two-pomeron phenomenology of DIS see also [30]. From the point of view of κ -factorization, the hard-to-soft diffusion is a unique mechanism by which an approximate constancy of $\Delta_{hard}(Q^2)$ derives from a very rapidly changing $\tau_{hard}(Q^2)$. Fourth, the same hard-to-soft diffusion provides a mechanism for the rise of the real photoabsorption cross section $\sigma^{\gamma p}$ in a model with the manifestly energy independent soft cross section. We emphasize that the hard-to-soft diffusion is a generic phenomenon and we do not see any possibility for decoupling of hard contribution from photoabsorption at $Q^2 = 0$.

We restricted ourselves to a purely phenomenological determination of differential gluon distributions from the experimental data on $F_{2p}(x, Q^2)$ which is sufficient for major applications of the κ -factorization technique. Whether the so-determined hard components of $\mathcal{F}(x, Q^2)$ and $G_D(x, Q^2)$ do satisfy the dynamical evolution equations and what is the onset of DGLAP regime will be addressed elsewhere.

IPI wishes to thank Prof. J.Speth for his hospitality at Forschungszentrum Jülich. This work was partly supported by the grant INTAS 97-30494.

References

- [1] V.N. Gribov and L.N. Lipatov, *Sov. J. Nucl. Phys.* **15** (1972) 438; L.N. Lipatov, *Sov. J. Nucl. Phys.* **20** (1974) 181; Yu.L. Dokshitser, *Sov. Phys. JETP* **46** (1977) 641; G. Altarelli and G. Parisi, *Nucl. Phys.* **B126** (1977) 298, for the review see R.G.Roberts, The structure of the proton. (Cambridge Univ. Press, 1990).
- [2] V.S.Fadin, E.A.Kuraev and L.N.Lipatov *Phys. Lett.* **B60** (1975) 50; E.A.Kuraev, L.N.Lipatov and V.S.Fadin, *Sov.Phys. JETP* **44** (1976) 443; **45** (1977) 199.
- [3] N.Nikolaev and B.G.Zakharov, *JETP* **78** (1994) 598; *Z. Phys.* **C64** (1994)631.
- [4] N.Nikolaev and B.G.Zakharov, *Phys. Lett.* **B332** (1994) 177; *Z. Phys.* **C53** (1992) 331.
- [5] N.N. Nikolaev, A.V. Pronyaev and B.G. Zakharov, *Phys. Rev.* **D59** 091501 (1999)
- [6] M. Bertini, M. Genovese, N.N. Nikolaev, A.V. Pronyaev and B.G. Zakharov, *Phys. Lett.* **B422**, 238 (1998)
- [7] E.V.Kuraev, N.N.Nikolaev, and B.G.Zakharov, *JETF Lett.* 68(1998) 667; I.P.Ivanov, N.N.Nikolaev, *Pis'ma ZhETF (JETP Lett.)* **69** (1999) 268
- [8] J. Nemchik, N.N. Nikolaev, E. Predazzi, B.G. Zakharov and V.R. Zoller, *J. Exp. Theor. Phys.* **86**, 1054 (1998)
- [9] N.N. Nikolaev, in: Hamburg 1998/1999, Monte Carlo generators for HERA physics, pp. 377-381. e-Print Archive: hep-ph/9905562.
- [10] M. Glueck, E. Reya, A. Vogt, *Eur.Phys.J.* **C5**:461-470,1998.
- [11] H.L. Lai, W.K. Tung, *Z.Phys.* **C74**:463-468,1997.
- [12] A.D. Martin, R.G. Roberts, W.J. Stirling, R.S. Thorne, *Phys.Lett.* **B443**:301-307,1998.
- [13] V. Barone, C. Pascaud and F. Zomer, *Eur. Phys. J.* **C12**, 243 (2000)
- [14] N.N. Nikolaev and V.R. Zoller, *JETP Lett.* **69**, 103 (1999); E. Gotsman, E. Levin, U. Maor and E. Naftali, *Nucl. Phys.* **B539**, 535 (1999)
- [15] H. Abramowicz and A. Caldwell, *Rev. Mod. Phys.* **71**, 1275 (1999); ZEUS Collab., J. Breitweg et al., *Eur. Phys. J.* **C7**, 609 (1999).
- [16] N.N. Nikolaev, B.G. Zakharov, *Phys. Lett.* **B327** (1994) 157.
- [17] N.N. Nikolaev, B.G. Zakharov, V.R. Zoller, *JETP Letters* **66** (1997) 138; N.N. Nikolaev, J. Speth and V.R. Zoller, *Phys. Lett.* **B473** (2000) 157.
- [18] V.M. Budnev, I.F. Ginzburg, G.V. Meledin and V.G. Serbo, *Phys. Rept.* **15**, 181 (1974)
- [19] N.N. Nikolaev and B.G. Zakharov, *Z. Phys.* **C49** (1991) 607.
- [20] N.N.Nikolaev and B.G.Zakharov, *Phys. Lett.* **B332** (1994) 184.

- [21] N.N. Nikolaev, B.G. Zakharov, V.R. Zoller , *JETP* **105** (1994) 1498.
- [22] N.N.Nikolaev and B.G.Zakharov, *Phys. Lett.* **B327** (1994) 157.
- [23] V.Barone, M.Genovese, N.N.Nikolaev, E.Predazzi and B.G.Zakharov, *Phys.Lett.* **B326** (1994) 161.
- [24] J.Nemchik, N.N.Nikolaev, E.Predazzi and B.G.Zakharov, *Phys. Lett.* **B374** (1966) 199.
- [25] . J.Nemchik, N.N.Nikolaev, E.Predazzi and B.G.Zakharov, *Z. Phys.* **C75** (1997) 71.
- [26] E. Meggiolaro, *Phys.Lett.* **B451** (1999) 414
- [27] J.Nemchik, N.N. Nikolaev and B.G. Zakharov, *Phys. Lett.* **B341** (1994) 228
- [28] V.N. Gribov, *Eur. Phys. J.* **C10** (1999) 71; D.V. Shirkov, *Phys. Atom. Nucl.* **62** (1999) 1928; Yu.L. Dokshitzer, G. Marchesini and B.R. Webber, *JHEP* **07** (1999) 012;
- [29] P.V.Landshoff and O.Nachtmann, *Z. Phys.* **C35** (1987) 405; H.G.Dosch, T.Gousset, G.Kulzinger and H.J.Pirner *Phys. Rev.* **D55** (1997) 2602.
- [30] A. Donnachie and P.V. Landshoff, *Phys.Lett.* **B437** (1998) 408
- [31] ZEUS coll., M. Derrick et al., *Z. Phys.* **C72** (1996) 399.
- [32] ZEUS coll., J. Breitweg et al., *Eur.Phys.J.* **C7** (1999) 609.
- [33] ZEUS coll., J. Breitweg et al., *Phys. Lett.* **B407** (1997) 432.
- [34] H1 coll., S. Aid et al., *Nucl. Phys.* **B470** (1996) 3.
- [35] H1 coll., C. Adloff et al., *Nucl. Phys.* **B497** (1996) 3.
- [36] E665 coll., M.R. Adams et al., *Phys. Rev.* **D54** (1996) 3006.
- [37] NMC coll., M. Arneodo et al., *Nucl. Phys.* **B483** (1997) 3.
- [38] ZEUS Collab., J.Breitweg et al., *Eur. Phys. J. C* **12** (2000) 35